zjv00813/zjv7521d13z | xppws | S=1 | 2/18/13 | 4:46 | 4/C Fig: 1,2,3,4,5,6 | Facing: 6-7 | ArtID: 02189-12 | NLM: research-article | CE: pmw

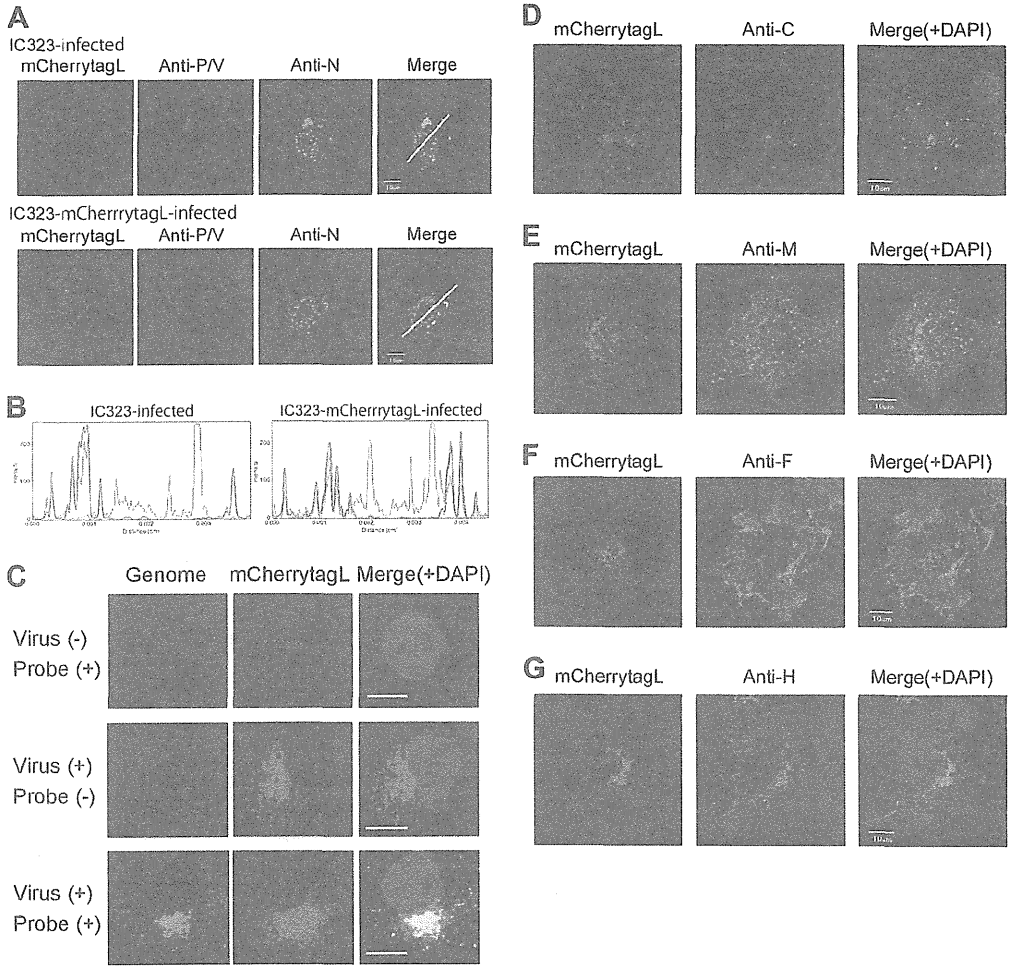

COLOR

FIG 2 Intracellular distributions of mCherry-tagged L protein and other viral proteins. (A) Vero/hSLAM cells were infected with IC323 or IC323-mCherrytagL, cultured for 2 days, and then analyzed by immunofluorescence and confocal microscopy. Red fluorescence indicates the mCherry-tagged L protein. The N and P/V proteins were detected with viral protein-specific primary antibodies and secondary antibodies conjugated with Alexa Fluor 488 (green) and Alexa Fluor 647 (blue, pseudocolor), respectively. The upper and lower panels show the results for IC323 and IC323-mCherrytagL, respectively. (B) RGB line profiles along the lines selected in panel A. The left and right panels show the data for IC323 and IC323-mCherrytagL, respectively. (C) Vero/hSLAM cells were infected with IC323-mCherrytagL, cultured for 2 days, and analyzed by fluorescence *in situ* hybridization assay. Lower panels show the result of MV-infected cells with a probe for genomic RNA. Green and red fluorescence indicates genomic RNA and mCherry-tagged L protein, respectively. Assays were also performed with mock-infected cells (upper panels). Middle panels show the result of MV-infected cells subjected to the fluorescence *in situ* hybridization assay without a probe for genomic RNA. Nuclei were counterstained with DAPI (blue). The scale bars indicate 10 μm. (D to G) Vero/hSLAM cells were infected with IC323-mCherrytagL, cultured for 2 days, and then analyzed by immunofluorescence and confocal microscopy. Red fluorescence indicates the mCherry-tagged L protein. The C (D), M (E), F (F), and H (G) proteins were detected with viral protein-specific primary antibodies and Alexa Fluor 488-conjugated secondary antibodies (green). Nuclei were counterstained with DAPI (blue). Scale bars indicate 10 μm.

Immunofluorescence and confocal microscopy. MV-infected cells were cultured for appropriate durations, fixed with phosphate-buffered saline (PBS) containing 4% paraformaldehyde, and then permeabilized with PBS containing 0.5% Triton X-100. Vero/hSLAM cells were inoculated and incubated for 2 days in the presence of the FBP to prevent cell-to-cell fusion before fixation. MDCK cells were fixed at 4 days postinfection (p.i.) in all experiments. The cells were then washed with PBS and incubated with a primary antibody, followed by incubation with a secondary antibody conjugated with Alexa Fluor 405, 488, 594, or 647. For counterstaining of the nuclei, the cells were incubated with DAPI. After the fluorescence staining, the cells were observed using an FV1000D Spectral Type confocal laser-scanning microscope (inverted microscope IX81) (Olympus, Tokyo, Japan). Data analysis was performed using FV10-ASW (Olympus) and ImageJ (National Institutes of Health, Bethesda, MD) software.

Time-lapse fluorescence microscopy. Cells were seeded on a 35-mm glass-based dish (Iwaki Glass, Tokyo, Japan), infected with an rMV, and cultured with the FBP for appropriate durations. The dish was placed in an incubation chamber installed in the FV1000D confocal laser-scanning microscope, in which the temperature and CO_2 concentration were maintained at 37°C and 5%, respectively. A total of 50 to 180 still images of the cells were taken at appropriate intervals using a 60×/1.35 NA oil objective (Olympus). Time intervals for acquisition of images were 10 min for Movie S1 and 1.1 s for Movies S2 to S5 in the supplemental material. Data analysis was performed using FV10-ASW and ImageJ software.

Fluorescence *in situ* hybridization assay. MV negative-strand genomic RNA was detected using the QuantiGene ViewRNA ISH cell assay kit (Affymetrix, Santa Clara, CA) and measles virus probe set (Affymetrix) that can hybridize to nucleotides 1489 to 2745 of the MV genome. Cells were applied to glass coverslips, infected with IC323-

zjv00813/zjv7521d13z | xppws | S=1 | 2/18/13 | 4:46 | 4/C Fig: 1,2,3,4,5,6 | Facing: 6-7 | ArtID: 02189-12 | NLM: research-article | CE: pmw

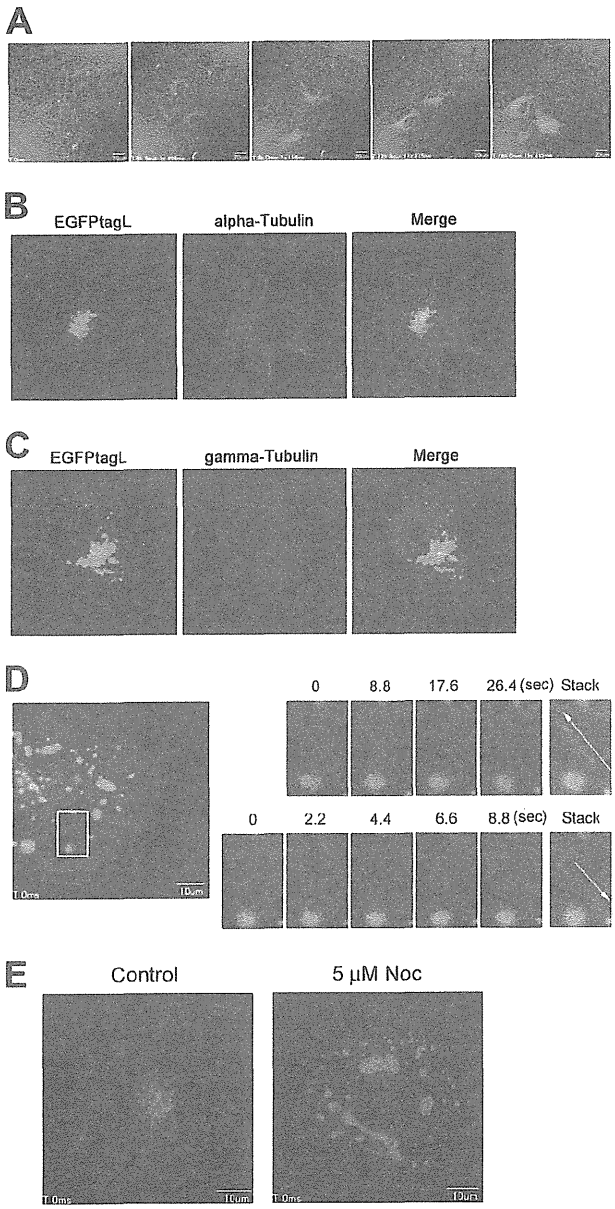

F1

F2

COLOR

FIG 3 Accumulation of the L protein at the MTOC in an MT-dependent manner. (A) Vero/hSLAM cells were infected with IC323-EGFPtagL, cultured for 24 h, and analyzed by time-lapse florescence microscopy. Five images taken at 4-h intervals are shown. Bars indicate 20 μm. (B and C) Vero/hSLAM cells were infected with IC323-EGFPtagL, cultured for 2 days, and analyzed by immunofluorescence and confocal microscopy. Green fluorescence indicates the EGFPtagL protein. α-Tubulin (B) and γ-tubulin (C) were detected with specific primary antibodies and Alexa Fluor 594-conjugated secondary antibodies (red). Nuclei were counterstained with DAPI (blue). (D) Vero/hSLAM cells were infected with IC323-EGFPtagL and transfected with pTagRFP-Tubulin. At 2 days p.i., the intracellular movement of EGFPtagL was analyzed by time-lapse fluorescence microscopy. A total of 150 still images were taken at 1.1-s intervals. The left panel shows the overall confocal image of the cells at the start of the time-lapse analysis. Green and red fluorescence indicates the EGFPtagL protein and TagRFP-tubulin, respectively. The scale bar indicates 10 μm. The right panels show enlarged time-lapse images and time-stacked images of the area indicated by the box in the left panel. The upper and lower panels show obliquely upward and downward movements of the EGFPtagL-containing dots, respectively, at different time points after starting the time-lapse analysis. Movements of the EGFPtagL fluorescence are indicated with white arrows in the time-stacked images. (E) Vero/hSLAM cells were infected with IC323-mCherrytagL. At 2 days p.i., the cells were treated with 5 μM nocodazole for 15 h (5 μM Noc) or left untreated (control). A total of 50 still images were taken at 1.1-s intervals. The panels show the overall confocal images of the cells at the start of the time-lapse analysis. Red fluorescence indicates the mCherrytagL protein. Scale bars indicate 10 μm.

mCherrytagL, and cultured for 2 days in the presence of the FBP. Cells were fixed in 4% formaldehyde solution, permeabilized, treated with protease, and hybridized according to the manufacturer's instructions. The cells were observed using an FV1000D Spectral Type confocal laser-scanning microscope (inverted microscope IX81). Data analysis was performed using FV10-ASW and ImageJ software.

RESULTS

Generation of rMVs encoding FLP-tagged L proteins. Previously, Duprex et al. (12) generated an Edmonston vaccine strain, rMV, encoding the L protein fused with EGFP in the variable hinge (H2) region. In the present study, based on the wild-type IC-B strain, rMVs encoding fluorescent protein (FLP)-tagged L proteins were generated. IC323-EGFPtagL and IC323-mCherrytagL encode the L protein fused with EGFP and mCherry, respectively, in the H2 region (12) (Fig. 1A). These rMVs were viable, and their replication kinetics was only slightly delayed compared with that of non-FLP-tagged IC323 in Vero/hSLAM cells (Fig. 1B and C). The growth of the Edmonston strain was more severely affected by the EGFP insertion in the H2 region (12). This difference may be attributed to the fact that the L protein of the IC323 strain exhibits higher activity than that of the Edmonston strain (25), and it may be more tolerant for the insertion than the Edmonston strain. The peak cell-associated and cell-free virus titers of IC323-EGFPtagL and IC323-mCherrytagL were comparable to those of non-FLP-tagged IC323 (Fig. 1B and C). These viruses efficiently produced syncytia expressing the FLP in monolayers of Vero/hSLAM cells (Fig. 1D) and were used for subsequent analyses of the transport and localization of the L protein during virus replication.

The RNP complex of MV accumulated at the perinuclear region in MV-infected Vero/hSLAM cells. To show the intracellular location and relationship of the L protein with other MV proteins, immunofluorescence assays were performed using a series of antibodies specific to each MV protein (Fig. 2). Previous studies indicated that the components of the RNP complex (N, P, and L proteins) are mostly colocalized and form dots of various sizes in the cytoplasm (13, 26). These observations were reexamined using IC323-EGFPtagL, IC323-mCherrytagL, and non-FLP-tagged IC323 to assess whether the FLP tagging had any untoward effects on the location of the RNP complex proteins. The EGFPtagL and mCherrytagL proteins were typically colocalized with the N and P/V proteins, with punctate fluorescence in the cytoplasm (Fig. 2A and B and data not shown), as reported previously (13). In these experiments, specific MAb against the N protein was used, while a rabbit polyclonal antibody raised against the common N terminus of the P and V proteins was used, since no antibody specific for the P protein was available. Thus, P/V indicates the P and/or V proteins. However, cells infected with the V protein-deficient rMV (MVΔV) (27) also showed a strong colocalization pattern of the N and P proteins (data not shown), indicating that the P protein colocalizes with the N and L proteins.

The localization patterns of the N and P/V proteins were sim-

zjv00813/zjv7521d13z | xppws | S=1 | 2/18/13 | 4:46 | 4/C Fig: 1,2,3,4,5,6 | Facing: 6-7 | ArtID: 02189-12 | NLM: research-article | CE: pmw

ilar among IC323-EGFPtagL-, IC323-mCherrytagL-, and IC323-infected cells (Fig. 2A and B and data not shown). These findings indicate that the FLP tags on the L protein hardly affected the distribution of the RNP complex proteins. Although punctate fluorescent areas indicating the N, P/V, and mCherrytagL (or EGFPtagL) proteins were distributed throughout the cytoplasm, they tended to concentrate at a perinuclear region (Fig. 2A and B and data not shown). In contrast to the N protein in the cytoplasm, the N protein located in the nucleus was not associated with the L and P/V proteins (Fig. 2A and B). The virus genome was also detected by fluorescence *in situ* hybridization assay (Fig. 2C). Consistent with the knowledge that MV undergoes its replication cycles entirely in the cytoplasm, the genome was detected exclusively in the cytoplasm that was concentrated at a perinuclear region, where the RNP complex proteins were accumulated (Fig. 2C). Additionally, the punctate signals of the L protein were colocalized with fluorescence signals for the virus genome (Fig. 2C). These data confirmed that the L protein signals represent the viral RNP complex.

Subsequently, the distributions of other viral proteins (C, M, F, and H) were analyzed using specific MAbs against these proteins, and representative single optical slice images are shown in Fig. 2D to G. The intracellular distribution patterns of these proteins were compared among IC323-EGFPtagL-, IC323-mCherrytagL-, and non-FLP-tagged IC323-infected cells and were found to be similar (data not shown). The C protein, which modulates viral RNA synthesis by interacting with the RNP complex, was almost perfectly colocalized with EGFPtagL and mCherrytagL (Fig. 2D and data not shown), as reported previously (13). The M protein was detected in both the cytoplasm and the nucleus in small dots and was partly associated with the plasma membrane (Fig. 2E). A portion of the M protein in the cytoplasm was colocalized with the L protein (Fig. 2E) that may represent the RNP-coating M protein destined to be incorporated into virions (28). Large parts of the F and H proteins were localized at the plasma membrane, and only fractions of these proteins in the cytoplasm were colocalized with the L protein in small dots (Fig. 2F and G).

The MV L protein is transported along MTs and concentrates at the microtubule-organizing center (MTOC) in MV-infected Vero/hSLAM cells. To clarify the overall trend of the L protein (EGFPtagL) movement, IC323-EGFPtagL-infected Vero/hSLAM cells were analyzed by time-lapse fluorescence microscopy. The data confirmed that, overall, the L protein moved to allow concentration at the perinuclear region (Fig. 3A; see Movie S1 in the supplemental material; data at 24 to 40 h p.i. are shown). The MTOC is known to be located at a perinuclear region in the center of cells. The minus ends of MTs face toward the MTOC, and the metronomic array of MTs is important for the directional transport of cellular proteins. MTs were detected using MAbs specific for α-tubulin (a major component of MTs) and γ-tubulin (a constituent of the minus ends of MTs anchored to the MTOC). The data revealed that the perinuclear region where the EGFPtagL protein was concentrated was the MTOC (Fig. 3B and C). To clarify the role of MTs in the transport, the movement of the EGFPtagL protein in cells expressing TagRFP (red FLP)-tagged α-tubulin was analyzed by time-lapse fluorescence microscopy. Each dot moved intermittently in various directions, showing a stop-start or zigzag movement along the MTs (Fig. 3D; see Movie S2 in the supplemental material). The EGFPtagL-containing dots moved in both directions along the MTs (Fig. 3D; see Movie S2), as observed

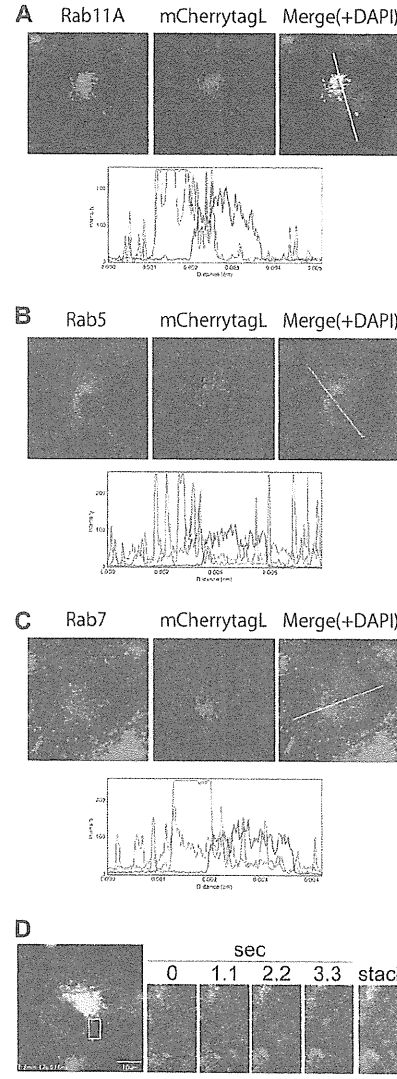

FIG 4 Colocalization and cotransport of mCherry-tagged L protein with EGFP-tagged Rab11A protein. (A–C) Vero/hSLAM cells constitutively expressing EGFP-Rab11A (A), -Rab5 (B), or -Rab7 (C) (Vero/hSLAM/EGFP-Rab cells) were infected with IC323-mCherrytagL. At 2 days p.i., the cells were fixed and analyzed by confocal microscopy. Green and red fluorescence indicates the EGFP-tagged Rab proteins and mCherrytagL protein, respectively. Nuclei were counterstained with DAPI (blue). The lower panels show the RGB line profiles along the selected lines in the merged images (upper right panels). (D) Vero/hSLAM/EGFP-Rab11A cells were infected with IC323-mCherrytagL. At 2 days p.i., the intracellular movements of EGFP-Rab11A and mCherrytagL were analyzed by time-lapse fluorescence microscopy. The left panel shows the overall confocal image of the cells at the start of the time-lapse analysis. Green and red fluorescence indicates the EGFP-Rab11A and mCherrytagL proteins, respectively. The right panels show enlarged time-lapse images of the area indicated by the box in the left panel. A representative series of images taken at 1.1-s intervals and a time-stacked image are shown. The movement of the mCherrytagL dots with EGFP-Rab11A is indicated by the white arrow in the time-stacked image.

for other viral and cellular proteins (29, 30). To confirm the dependency on MTs, IC323-mCherrytagL-infected cells were treated with 5 μM nocodazole, an MT-disrupting agent, or left untreated as a control, and the movement of the mCherrytagL-

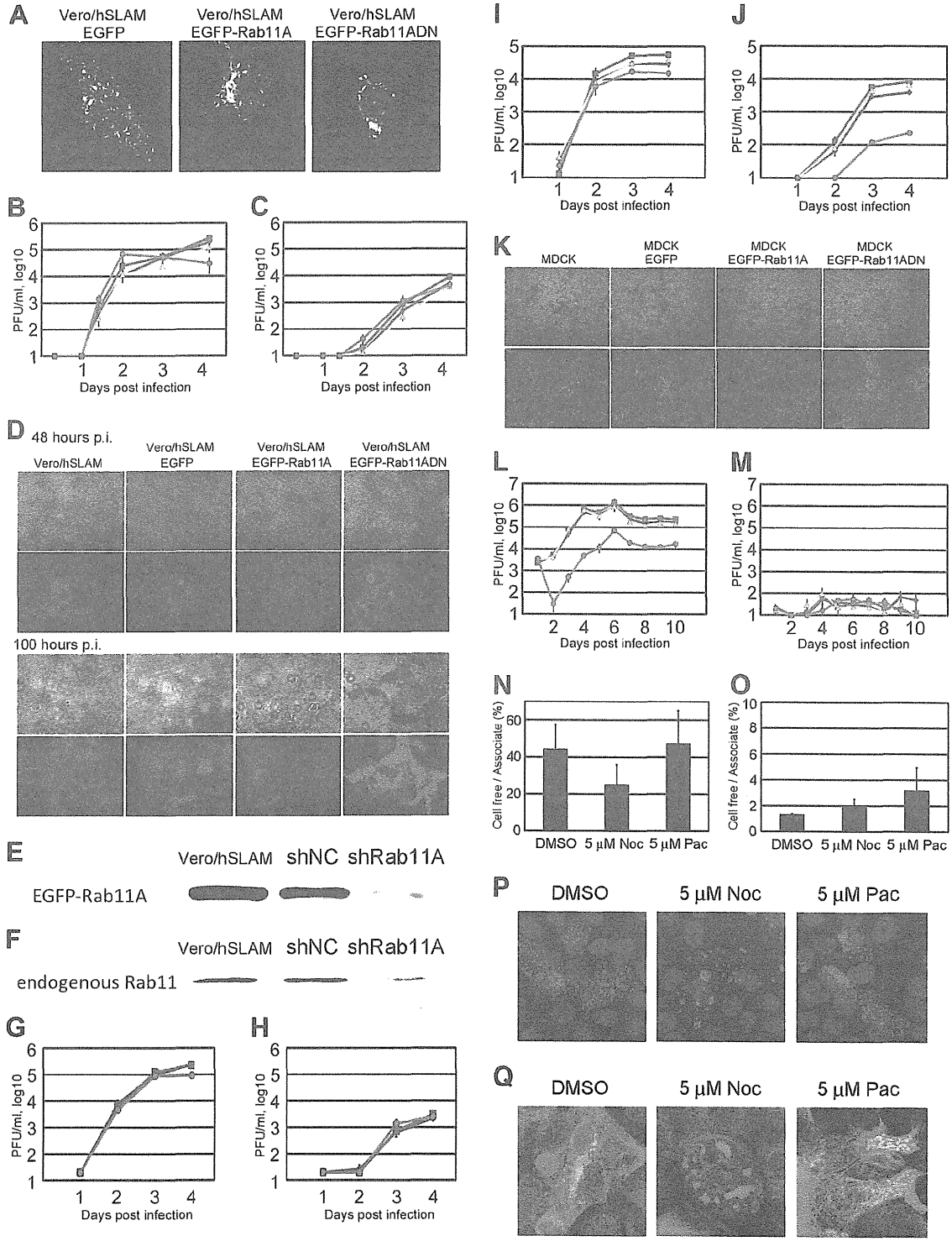

COLOR

FIG 5 Growth kinetics of the IC323-AddmCherry virus in Rab11ADN-expressing Vero/hSLAM or MDCK cells. (A) Vero/hSLAM cells constitutively expressing EGFP, EGFP-Rab11A, or EGFP-Rab11ADN were infected with IC323, cultured for 1 day, and analyzed by immunofluorescence and confocal microscopy. The N protein was detected by indirect immunofluorescence assay. (B to D) Vero/hSLAM cells constitutively expressing EGFP, EGFP-Rab11A, or EGFP-Rab11ADN were infected with IC323-AddmCherry at an MOI of 0.01. At various time points, the cells and culture medium were harvested separately, and the PFU in both samples were determined. The data for the cell-associated and cell-free titers are plotted in panels B and C, respectively. The data represent the means ± standard deviations of results from triplicate samples. The blue, red, yellow, and green lines indicate the data for Vero/hSLAM, Vero/hSLAM/EGFP, Vero/hSLAM/EGFP-Rab11A, and Vero/hSLAM/EGFP-Rab11ADN, respectively. In panel D, representative CPEs at 48 and 100 h p.i. are shown. Red fluorescence indicates the virus-derived mCherry expression. (E) Vero/hSLAM cells constitutively expressing negative-control shRNA (shNC) or shRNA against Rab11A mRNA

containing dots was analyzed by time-lapse fluorescence microscopy. In the control cells, the mCherrytagL-containing dots were transported efficiently throughout the cytoplasm (see Movie S3 in the supplemental material). On the other hand, the mCherrytagL-containing dots no longer moved actively in the nocodazole-treated cells (see Movie S4 in the supplemental material). It was also found that the accumulation of mCherrytagL at the perinuclear region was disrupted by treatment with 5 μM nocodazole (Fig. 3E). These findings indicate that the MV RNP complexes are transported to and concentrated at the MTOC in an MT-dependent manner.

The L protein moves along with Rab11A-containing REs. To determine the roles of transport vehicles in the trafficking of the RNP complex of MV, the intracellular distributions of mCherrytagL protein and EGFP-tagged Rab (EGFP-Rab) proteins were analyzed in the same cells. Rab proteins contribute to the synthesis, transport, and function of specific endosomes and are used as endosome markers (31). Recent studies showed that specific endosomes are associated with viral protein transport along MTs (7, 9, 10). Vero/hSLAM cells constitutively expressing EGFP-Rab5, -Rab7, or -Rab11A (Vero/hSLAM/EGFP-Rab cells) were generated and infected with IC323-mCherrytagL. Rab5, Rab7, and Rab11A are markers for early endosomes, late endosomes, and REs, respectively (31). In cells infected with IC323-mCherrytagL, the mCherrytagL-containing dots were mostly co-
F4 localized with EGFP-Rab11A (Fig. 4A). On the other hand, the signals were poorly associated with the EGFP signals of Rab5 and Rab7 (Fig. 4B and C). These findings suggest that the MV RNP complex is associated with REs. The intracellular transport of the L protein in association with Rab11A was analyzed by time-lapse fluorescence microscopy. The data clearly showed that mCherrytagL was transported along with Rab11A (Fig. 4D; see Movie S5 in the supplemental material). Therefore, our findings suggest that REs function as vehicles for transport of the MV RNP complex.

Rab11A plays a role for efficient MV release from polarized epithelial cells. A dominant negative form of Rab11A (Rab11ADN) having a S25N mutation was used to perturb the functions of endogenous Rab11A. The distribution pattern of viral RNP complex in Vero/hSLAM/EGFP-Rab11ADN cells was similar to those in Vero/hSLAM/EGFP and Vero/hSLAM/EGFP-Rab11A cells (Fig. 5A). In subsequent experiments, IC323-Addm- F5
Cherry encoding a red FLP (mCherry) in the additional independent transcription unit between the H and L genes was used to visualize MV-infected cells. At 2 days p.i., both the cell-associated and cell-free virus titers in Vero/hSLAM/EGFP-Rab11ADN cells were unaffected or were slightly higher than those in other cells (Fig. 5B and C). Vero/hSLAM/EGFP-Rab11ADN cells showed a stronger cytopathic effect (CPE) than the other cells, and at 100 h p.i., the cell-associated virus titer in Vero/hSLAM/EGFP-Rab11ADN cells was markedly decreased (Fig. 5B and D). Knockdown of Rab11A expression also hardly affected MV growth in Vero/hSLAM cells (Fig. 5E to H). These data show that, although the transport of MV RNP complex is mediated by Rab11A-positive REs, it is not critical for MV growth in Vero/hSLAM cells.

Similar virus growth assays were conducted in polarized epithelial cells, since directional budding of MV was previously reported (6, 32) and the locations and functions of REs differ between nonpolarized and polarized epithelial cells (31). MDCK cells are well-studied polarized epithelial cells. We found that MDCK cells were to some extent susceptible to the IC323 strain infection, as observed from the infection with the laboratory-adapted Edmonston strain (6). Using Vero cells expressing canine and human nectin4 (33, 34), we found that canine nectin4 functions as an MV receptor as well as human nectin4 (data not shown). It was recently reported that MDCK cells express canine nectin4 (35). Thus, MV likely uses this epithelial cell molecule (canine nectin4) to enter MDCK cells. As shown in Fig. 5I and J, the cell-free virus titer of IC323-AddmCherry in MDCK/EGFP-Rab11ADN cells was ~20-fold lower than those in MDCK/EGFP, MDCK/EGFP-Rab11A, and parental MDCK cells, while the cell-associated virus titer in MDCK/EGFP-Rab11ADN cells was comparable to those in the other cells. The CPE was weak in the MDCK-derived cell lines and similar among the cells (Fig. 5K). These findings suggest that Rab11A is necessary for efficient MV release into the culture medium from MDCK cells. The kinetics of the MV release from these MDCK-derived cell lines was reexamined on transwell filters, since selective MV release from the apical surface was previously described under this culture condition (6). The formation of an electrically tight monolayer was confirmed

(shRab11A) were transfected with pMXsIP-EGFP-Rab11A. At 2 days posttransfection, EGFP-Rab11A expression levels were analyzed by Western blotting. (F) Vero/hSLAM cells constitutively expressing shNC or shRab11A were lysed and endogenous Rab11 expression was analyzed by Western blotting. (G and H) Vero/hSLAM cells constitutively expressing shNC or shRab11A were infected with IC323-AddmCherry at an MOI of 0.01. At various time points, PFU in cells (G) and culture medium (H) were determined. The data represent the means ± standard deviations of results from triplicate samples. The blue, red, and green lines indicate the data for Vero/hSLAM, Vero/hSLAM/shNC, and Vero/hSLAM/shRab11A, respectively. (I to K) MDCK cells constitutively expressing EGFP, EGFP-Rab11A, or EGFP-Rab11ADN were plated on 24-well plates and immediately infected with IC323-AddmCherry at an MOI of 0.2. At various time points, the cells and culture medium were harvested separately, and the PFU in both samples were determined. The data for the cell-associated and cell-free titer are plotted in panels I and J, respectively. The data represent the means ± standard deviations of results from triplicate samples. The blue, red, yellow, and green lines indicate the data for MDCK, MDCK/EGFP, MDCK/EGFP-Rab11A, and MDCK/EGFP-Rab11ADN, respectively. In panel K, representative CPEs at 4 days p.i. are shown. Red fluorescence indicates the virus-derived mCherry expression. (L and M) MDCK cells constitutively expressing EGFP, EGFP-Rab11A, or EGFP-Rab11ADN were seeded on transwell filters with 0.4-μm pores and immediately infected with IC323-AddmCherry at an MOI of 0.2. At various time points, the apical and basolateral media were harvested separately, and the PFU in both samples were determined. The data for the apical and basolateral titers are plotted in panels L and M, respectively. The data represent the means ± standard deviations of results from triplicate samples. The blue, red, yellow, and green lines indicate the data for MDCK, MDCK/EGFP, MDCK/EGFP-Rab11A, and MDCK/EGFP-Rab11ADN, respectively. (N and O) MDCK (N) and Vero/hSLAM (O) cells were infected with IC323-AddmCherry at MOIs of 0.2 and 0.01, respectively. At 4 and 2 days p.i., MDCK cells and Vero cells, respectively, were treated with reagents (5 μM nocodazole [5 μM Noc], 5 μM paclitaxel [5 μM Pac], or dimethyl sulfoxide [DMSO] [as vehicle control]) for 1 day. PFU counts in cells and culture medium were determined. The ratios of cell-free virus titer to cell-associated virus titer are plotted. The data represent the means ± standard deviations of results from triplicate samples. (P and Q) MDCK (P) and Vero/hSLAM (Q) cells, which were transfected with pAcGFP1-Tubulin, were infected with IC323-mCherrytagL at MOIs of 0.2 and 0.1, respectively. At 4 and 2 days p.i., MDCK cells and Vero/hSLAM cells, respectively, were treated with reagents for 1 day. Then, cells were fixed and nuclei were stained with DAPI (blue). Z-stacks of images were acquired by confocal microscopy. Green (Q) and red (P and Q) fluorescence indicates the AcGFP-tagged α-tubulin and mCherrytagL protein, respectively. The Z-projection images of the maximum intensities are shown.

zjv00813/zjv7521d13z | xppws | S=1 | 2/18/13 | 4:46 | 4/C Fig: 1,2,3,4,5,6 | Facing: 6-7 | ArtID: 02189-12 | NLM: research-article | CE: pmw

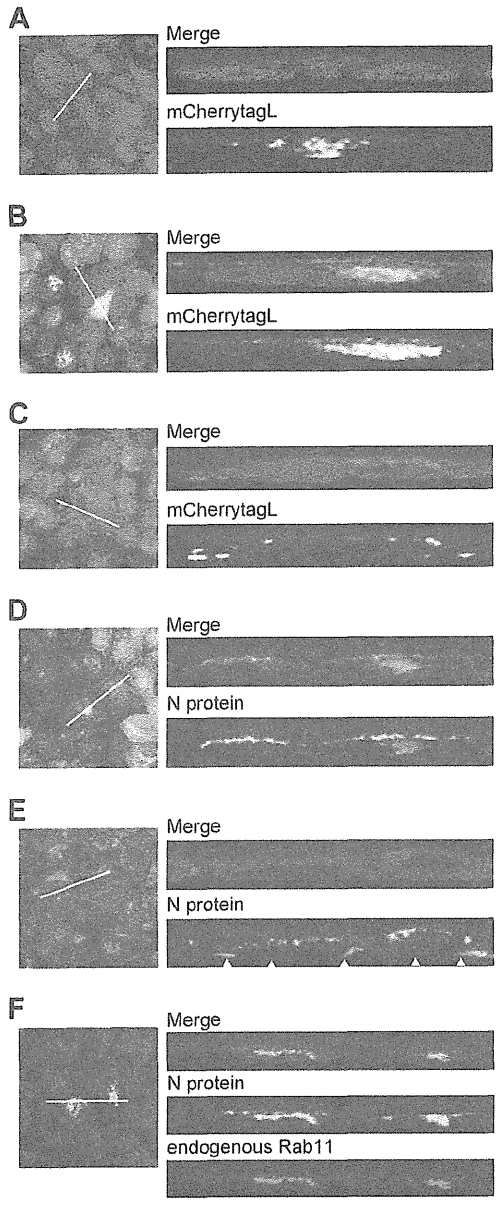

F6

COLOR

FIG 6 Intracellular localizations of the MV RNP complex and Rab11 in MDCK cells. (A to C) MDCK/EGFP (A), MDCK/EGFP-Rab11A (B), and MDCK/EGFP-Rab11ADN (C) cells were infected with IC323-mCherrytagL at an MOI of 0.2. At 4 days p.i., the cells were fixed and their nuclei were stained with DAPI (blue). Z-stacks of images were acquired by confocal microscopy. Green and red fluorescence in the merged images indicates the EGFP-tagged proteins and mCherrytagL protein, respectively. The left panels show Z-projection images of the maximum intensities, and the right panels show reconstituted images of the XZ plane along the lines in the left panels. (D and E) MDCK/EGFP-Rab11A (D) and MDCK/EGFP-Rab11ADN (E) cells were infected with IC323 at an MOI of 0.2. At 4 days p.i., the cell membrane was stained with CM-Dil (red in the merged images) and the cells were fixed for analyses by immunofluorescence and confocal microscopy. Green fluorescence in the merged images indicates the EGFP-tagged proteins. The N protein was detected with a specific primary antibody and an Alexa Fluor 405-conjugated secondary antibody (blue in the merged images). The left and right panels show Z-projection images and reconstituted images of the XZ plane, respectively, as shown in panels A to C. Arrowheads in panel E indicate the accumulation of the N proteins at the bottom of the cytoplasm. (F) MDCK cells were infected with IC323 at an MOI of 0.2. At 4 days p.i., the cell membrane was stained with CM-Dil (red in the merged images) and the cells were fixed for analyses by immunofluorescence and confocal microscopy. The N protein and endogenous Rab11 were detected with specific primary antibodies and secondary antibodies conjugated with Alexa Fluor 405 (blue in the merged images) and Alexa Fluor 488 (green), respectively. The left and right panels show Z-projection images and reconstituted images of the XZ plane, respectively, as shown in panels A to C.

daily by measuring the transepithelial resistance (36). As expected, MV was released exclusively from the apical side (Fig. 5L and M). In the MDCK/EGFP-Rab11ADN cell culture, the MV titer in the apical culture medium was 10- to 100-fold lower than those in the other three cell cultures (Fig. 5L and M).

We also analyzed effects of MT disrupting (nocodazole) and stabilizing (paclitaxel) drugs on MV release from Vero/hSLAM and MDCK cells. Nocodazole treatment partially affected MV release from MDCK cells but not from Vero/hSLAM cells (Fig. 5N to Q). Although there was only a partial effect, it should be considered that after a 4-day-incubation period, MV-infected MDCK cells were incubated with nocodazole for only 1 day prior to virus harvest, since a long incubation with nocodazole was highly toxic to cells. Paclitaxel treatment showed little, if any, effect on MV release from these cells (Fig. 5N to Q). These data suggest that Rab11A-positive REs specifically function to guide the MV RNP complex to the apical direction (toward the minus end of MTs) of polarized epithelial cells for efficient virus release from the apical membrane. In Vero/hSLAM cells, the MV RNP complex was concentrated at the MTOC (the minus end of MTs). Consistent with these data, the ratio of cell-free virus titers (released virus particles) to cell-associated virus titers in Vero/hSLAM cells was much lower than that in MDCK cells, even in the absence of nocodazole (Fig. 5N and O).

The MV RNP complex accumulates at the apical membrane and the apical recycling compartment (ARC) via functions of Rab11A. The orientation of MTs and vesicular transport system have been shown to differ between polarized epithelial cells and nonpolarized cells (31, 37). To determine the location of the MV RNP complex in MDCK cells and examine the effects of Rab11ADN, imaging analyses were performed using a confocal laser-scanning microscope. In MDCK/EGFP cells, mCherrytagL was accumulated at or beneath the apical plasma membrane and at a specific intracellular region (Fig. 6A). The data for MDCK/EGFP-Rab11A cells demonstrated that the mCherrytagL located at the apical membrane and the intracellular region was mostly colocalized with EGFP-Rab11A, a marker of the ARC in polarized epithelial cells (31) (Fig. 6B). Therefore, the intracellular region was likely to be the ARC. On the other hand, in MDCK/EGFP-Rab11ADN cells, mCherrytagL was poorly accumulated at the apical membrane, and a region corresponding to the ARC was not detected (Fig. 6C). Instead, mCherrytagL was concentrated in other regions at the bottom of the cytoplasm (Fig. 6C). Similar imaging analyses were performed using a non-FLP-tagged IC323 virus and a MAb against the N protein. For this assay, CM-Dil, a highly lipophilic carbocyanine dye, was used to visualize the overall cell morphology. In MDCK/EGFP-Rab11A cells, the N protein was accumulated beneath the apical membrane and at the ARC and was colocalized with EGFP-Rab11A (Fig. 6D). In MDCK/EGFP-Rab11ADN cells, the N protein was detected throughout the cell and was not concentrated at the apical membrane or the ARC (Fig. 6E). Finally, the colocalization of the N protein with

endogenous Rab11 was analyzed in IC323-infected MDCK cells; that is, only unmodified (natural) proteins were evaluated in this experiment. The data demonstrated that the N protein was accumulated beneath the apical plasma membrane and at the ARC and was colocalized with endogenous Rab11 proteins (Fig. 6F). Taken together, these findings indicate that the RNP complex of MV is accumulated at the apical membrane and the ARC in polarized epithelial cells by a mechanism dependent on Rab11A-positive REs.

DISCUSSION

Measles is an airborne disease, and MV is evidently one of the most transmissible pathogens. MV must have mechanisms to shed progeny viruses efficiently. Recent findings for MV infection of polarized epithelial cells and selective budding from the apical membrane can, in part, nicely explain the efficient virus shedding *in vivo*. However, the intracellular events for trafficking of MV proteins that lead to virus shedding from the apical membrane remain largely unknown.

Much information about the intracellular trafficking of cellular proteins and viral proteins has been obtained using FLP technology (38). Although an rMV expressing the L protein fused with EGFP was generated previously (12, 13), detailed analyses of the trafficking of the MV L protein have not been conducted. The present data obtained using FLP-tagged L proteins clearly demonstrated that, similarly to SeV and IAV (7, 9, 10), the MV RNP complex was transported in a MT-dependent manner and associated with Rab11A-positive REs. MTs have a polar nature, and the minus ends of most MTs are anchored in the MTOC in nonpolarized cells and directed toward the apical membrane in polarized epithelial cells (37, 39). Previous papers showed that the polar nature of MTs is important for the directional transport of some viral proteins (7, 9, 11, 37, 40) and that transport using REs is critical for particle production of IAV at the cell surface (8, 10). It is also noteworthy that respiratory syncytial virus requires an RE-mediated protein sorting system for efficient budding from the apical membrane in polarized epithelial cells (41, 42). Importantly, our data revealed that the functions of Rab11A are critical only for apical release of MV from polarized epithelial cells and not for virus production in nonpolarized Vero/hSLAM cells. Even destruction of the MTs by nocodazole did not significantly affect virus production in Vero/hSLAM cells. Therefore, Rab11A- and RE-dependent RNP transport is not a general requirement for MV replication and particle production but is specifically required for the apical release of MV particles from polarized epithelial cells. The work will raise questions in the field regarding differences in sorting mechanisms between MV, respiratory syncytial virus, SeV, and IAV.

These observations may, in part, be inconsistent with the previous finding by Berghall et al. (43) that nocodazole treatment of Vero cells causes a reduction in MV progeny production. However, nocodazole has a broad-spectrum effect, because the MTs are important for almost all cellular activities, including cell division, intracellular signal transduction, and cell metabolism. Therefore, the effects of nocodazole on MV replication might be affected by subtle differences in the cell conditions. Similarly, the importance of accumulation of the MV RNP complex at the MTOC in Vero/hSLAM cells remains unclear, because nonpolarized epithelial cells are unnatural host cells for MV, and it is also largely unclear whether the accumulation of viral proteins, called viral inclusion, at the perinuclear site close to the MTOC is beneficial to the virus or the host cell (44). The MV RNP was accumulated beneath the apical membrane and at the ARC in polarized epithelial cells, a natural target *in vivo*.

Our data show that the selective progeny virus release from the apical membrane (5, 6, 32) is at least partly driven by the apical transport of the RNP complex. However, other molecular mechanisms and the contributions of other viral proteins remain to be investigated. The two glycoproteins, H and F, were selectively transported to the basolateral surface in MDCK cells, and the M protein redirected the H and F proteins to the apical surface in MV-infected cells (6, 45). However, the M protein expressed alone using a plasmid was homogeneously distributed throughout the cell and did not accumulate as large clusters at the cell surface in MDCK cells (46). Thus, the roles of the M protein in the apical virus release are still uncertain. It is necessary to address which virus components or cellular proteins are necessary for MV release from the apical membrane. Consistent with our imaging analysis data that the L protein was often associated with the M protein, a recent study showed that the MV M protein mainly functions to coat the RNP complex and not for association with the viral envelope (28). For IAV, the viral glycoproteins and matrix proteins are transported by mechanisms distinct from that of the viral RNP complex (47) and the process of the RNP complex transport is mediated by direct or indirect interactions between the viral polymerase complex (PB1, PB2, and PA complex) and Rab11 (8, 10, 48). The impacts of the M protein and H and F glycoproteins on the transport of the MV RNP complex are now under investigation in our laboratory.

It is of interest to analyze the intracellular transport of MV proteins in different cell types, including lymphocytes and neurons, because they are also *in vivo* target cells of MV, and MV infection of these cells is associated with immunosuppression and encephalitis. Duprex and colleagues demonstrated cell-to-cell spread of MV in astrocytoma cells, and MV infection caused disruption of the glial-fibrillary-acidic protein filament but not MTs (49, 50). The implementation of these studies in various cell types is expected to elucidate the molecular mechanisms of MV pathogenicity. Interestingly, cells in the central nervous system possess differently orientated MTs and distinct cell polarity (37).

In conclusion, the data obtained in the present study demonstrate that the MV RNP complex is transported in an MT-dependent manner together with Rab11A-containing REs to become accumulated at the apical membrane and the ARC. This RE-mediated RNP transport is dispensable for virus production in nonpolarized cells but critical for virus shedding from the apical membrane of polarized epithelial cells. These data provide evidence for the regulated intracellular trafficking events of the MV RNP complex that drive the viral shedding from polarized epithelial cells.

ACKNOWLEDGMENTS

We thank T.A. Sato and N. Ito for providing the MAbs against the N, M, F, and H proteins of MV and the BHK/T7-9 cells, respectively. We also thank M. Shimojima and T. Kitamura for providing PLAT-gp cells, pMXs-IP, and pCVSV-G.

This work was supported by grants from the Ministry of Education, Culture, Sports, Science and Technology, the Ministry of Health, Labor and Welfare of Japan, and the Takeda Science Foundation.

REFERENCES

1. **Griffin DE.** 2007. Measles virus, p 1551–1585. *In* Knipe DM, Howley PM, Griffin DE, Lamb RA, Martin MA, Roizman B, Straus SE (ed), Fields virology, 5th ed. Lippincott Williams & Wilkins, Philadelphia, PA.
2. **Leonard VH, Sinn PL, Hodge G, Miest T, Devaux P, Oezguen N, Braun W, McCray PB, Jr, McChesney MB, Cattaneo R.** 2008. Measles virus blind to its epithelial cell receptor remains virulent in rhesus monkeys but cannot cross the airway epithelium and is not shed. J. Clin. Invest. **118**: 2448–2458.
3. **Muhlebach MD, Mateo M, Sinn PL, Prufer S, Uhlig KM, Leonard VH, Navaratnarajah CK, Frenzke M, Wong XX, Sawatsky B, Ramachandran S, McCray PB, Jr, Cichutek K, von Messling V, Lopez M, Cattaneo R.** 2011. Adherens junction protein nectin-4 is the epithelial receptor for measles virus. Nature **480**:530–533.
4. **Noyce RS, Bondre DG, Ha MN, Lin LT, Sisson G, Tsao MS, Richardson CD.** 2011. Tumor cell marker PVRL4 (nectin 4) is an epithelial cell receptor for measles virus. PLoS Pathog. 7:e1002240. doi:10.1371/journal.ppat.1002240.
5. **Blau DM, Compans RW.** 1995. Entry and release of measles virus are polarized in epithelial cells. Virology **210**:91–99.
6. **Maisner A, Klenk H, Herrler G.** 1998. Polarized budding of measles virus is not determined by viral surface glycoproteins. J. Virol. 72:5276–5278.
7. **Chambers R, Takimoto T.** 2010. Trafficking of Sendai virus nucleocapsids is mediated by intracellular vesicles. PLoS One 5:e10994. doi:10.1371/journal.pone.0010994.
8. **Eisfeld AJ, Kawakami E, Watanabe T, Neumann G, Kawaoka Y.** 2011. RAB11A is essential for transport of the influenza virus genome to the plasma membrane. J. Virol. 85:6117–6126.
9. **Momose F, Kikuchi Y, Komase K, Morikawa Y.** 2007. Visualization of microtubule-mediated transport of influenza viral progeny ribonucleoprotein. Microbes Infect. 9:1422–1433.
10. **Momose F, Sekimoto T, Ohkura T, Jo S, Kawaguchi A, Nagata K, Morikawa Y.** 2011. Apical transport of influenza A virus ribonucleoprotein requires Rab11-positive recycling endosome. PLoS One 6:e21123. doi:10.1371/journal.pone.0021123.
11. **Das SC, Nayak D, Zhou Y, Pattnaik AK.** 2006. Visualization of intracellular transport of vesicular stomatitis virus nucleocapsids in living cells. J. Virol. 80:6368–6377.
12. **Duprex WP, Collins FM, Rima BK.** 2002. Modulating the function of the measles virus RNA-dependent RNA polymerase by insertion of green fluorescent protein into the open reading frame. J. Virol. 76:7322–7328.
13. **Nakatsu Y, Takeda M, Ohno S, Shirogane Y, Iwasaki M, Yanagi Y.** 2008. Measles virus circumvents the host interferon response by different actions of the C and V proteins. J. Virol. 82:8296–8306.
14. **Nakatsu Y, Takeda M, Iwasaki M, Yanagi Y.** 2009. A highly attenuated measles virus vaccine strain encodes a fully functional C protein. J. Virol. 83:11996–12001.
15. **Prasain N, Alexeyev M, Balczon R, Stevens T.** 2009. Soluble adenylyl cyclase-dependent microtubule disassembly reveals a novel mechanism of endothelial cell retraction. Am. J. Physiol. Lung Cell. Mol. Physiol. 297: L73–L83.
16. **Serio G, Margaria V, Jensen S, Oldani A, Bartek J, Bussolino F, Lanzetti L.** 2011. Small GTPase Rab5 participates in chromosome congression and regulates localization of the centromere-associated protein CENP-F to kinetochores. Proc. Natl. Acad. Sci. U. S. A. **108**:17337–17342.
17. **Kitamura T, Koshino Y, Shibata F, Oki T, Nakajima H, Nosaka T, Kumagai H.** 2003. Retrovirus-mediated gene transfer and expression cloning: powerful tools in functional genomics. Exp. Hematol. **31**:1007–1014.
18. **Ono N, Tatsuo H, Hidaka Y, Aoki T, Minagawa H, Yanagi Y.** 2001. Measles viruses on throat swabs from measles patients use signaling lymphocytic activation molecule (CDw150) but not CD46 as a cellular receptor. J. Virol. 75:4399–4401.
19. **Ito N, Takayama-Ito M, Yamada K, Hosokawa J, Sugiyama M, Minamoto N.** 2003. Improved recovery of rabies virus from cloned cDNA using a vaccinia virus-free reverse genetics system. Microbiol. Immunol. 47:613–617.
20. **Morita S, Kojima T, Kitamura T.** 2000. Plat-E: an efficient and stable system for transient packaging of retroviruses. Gene Ther. 7:1063–1066.
21. **Takeda M, Takeuchi K, Miyajima N, Kobune F, Ami Y, Nagata N, Suzaki Y, Nagai Y, Tashiro M.** 2000. Recovery of pathogenic measles virus from cloned cDNA. J. Virol. 74:6643–6647.
22. **Seki F, Yamada K, Nakatsu Y, Okamura K, Yanagi Y, Nakayama T, Komase K, Takeda M.** 2011. The SI strain of measles virus derived from a patient with subacute sclerosing panencephalitis possesses typical genome alterations and unique amino acid changes that modulate receptor specificity and reduce membrane fusion activity. J. Virol. 85:11871–11882.
23. **Nakatsu Y, Takeda M, Ohno S, Koga R, Yanagi Y.** 2006. Translational inhibition and increased interferon induction in cells infected with C protein-deficient measles virus. J. Virol. 80:11861–11867.
24. **Tahara M, Takeda M, Yanagi Y.** 2007. Altered interaction of the matrix protein with the cytoplasmic tail of hemagglutinin modulates measles virus growth by affecting virus assembly and cell-cell fusion. J. Virol. 81: 6827–6836.
25. **Takeda M, Ohno S, Tahara M, Takeuchi H, Shirogane Y, Ohmura H, Nakamura T, Yanagi Y.** 2008. Measles viruses possessing the polymerase protein genes of the Edmonston vaccine strain exhibit attenuated gene expression and growth in cultured cells and SLAM knock-in mice. J. Virol. 82:11979–11984.
26. **Iwasaki M, Takeda M, Shirogane Y, Nakatsu Y, Nakamura T, Yanagi Y.** 2009. The matrix protein of measles virus regulates viral RNA synthesis and assembly by interacting with the nucleocapsid protein. J. Virol. 83: 10374–10383.
27. **Ikegame S, Takeda M, Ohno S, Nakatsu Y, Nakanishi Y, Yanagi Y.** 2010. Both RIG-I and MDA5 RNA helicases contribute to the induction of alpha/beta interferon in measles virus-infected human cells. J. Virol. 84: 372–379.
28. **Liljeroos L, Huiskonen JT, Ora A, Susi P, Butcher SJ.** 2011. Electron cryotomography of measles virus reveals how matrix protein coats the ribonucleocapsid within intact virions. Proc. Natl. Acad. Sci. U. S. A. **108**: 18085–18090.
29. **Mallik R, Gross SP.** 2004. Molecular motors: strategies to get along. Curr. Biol. 14:R971–R982.
30. **Welte MA.** 2004. Bidirectional transport along microtubules. Curr. Biol. 14:R525–R537.
31. **Somsel Rodman J, Wandinger-Ness A.** 2000. Rab GTPases coordinate endocytosis. J. Cell Sci. 113(Part 2):183–192.
32. **Tahara M, Takeda M, Shirogane Y, Hashiguchi T, Ohno S, Yanagi Y.** 2008. Measles virus infects both polarized epithelial and immune cells by using distinctive receptor-binding sites on its hemagglutinin. J. Virol. 82: 4630–4637.
33. **Otsuki N, Sekizuka T, Seki F, Sakai K, Kubota T, Nakatsu Y, Chen S, Fukuhara H, Maenaka K, Yamaguchi R, Kuroda M, Takeda M.** 2013. Canine distemper virus with the intact C protein has the potential to replicate in human epithelial cells by using human nectin4 as a receptor. Virology 435:485–492.
34. **Pratakpiriya W, Seki F, Otsuki N, Sakai K, Fukuhara H, Katamoto H, Hirai T, Maenaka K, Techangamsuwan S, Lan NT, Takeda M, Yamaguchi R.** 2012. Nectin4 is an epithelial cell receptor for canine distemper virus and involved in neurovirulence. J. Virol. **86**:10207–10210.
35. **Noyce RS, Delpeut S, Richardson CD.** 2013. Dog nectin-4 is an epithelial cell receptor for canine distemper virus that facilitates virus entry and syncytia formation. Virology 436:210–220.
36. **Yu AS, Enck AH, Lencer WI, Schneeberger EE.** 2003. Claudin-8 expression in Madin-Darby canine kidney cells augments the paracellular barrier to cation permeation. J. Biol. Chem. 278:17350–17359.
37. **Dohner K, Nagel CH, Sodeik B.** 2005. Viral stop-and-go along microtubules: taking a ride with dynein and kinesins. Trends Microbiol. 13:320–327.
38. **Campbell EM, Hope TJ.** 2008. Live cell imaging of the HIV-1 life cycle. Trends Microbiol. 16:580–587.
39. **Li Q, Joshi HC.** 1995. Gamma-tubulin is a minus end-specific microtubule binding protein. J. Cell Biol. 131:207–214.
40. **Greber UF, Way M.** 2006. A superhighway to virus infection. Cell 124: 741–754.
41. **Brock SC, Goldenring JR, Crowe JE, Jr.** 2003. Apical recycling systems regulate directional budding of respiratory syncytial virus from polarized epithelial cells. Proc. Natl. Acad. Sci. U. S. A. **100**:15143–15148.
42. **Utley TJ, Ducharme NA, Varthakavi V, Shepherd BE, Santangelo PJ, Lindquist ME, Goldenring JR, Crowe JE, Jr.** 2008. Respiratory syncytial virus uses a Vps4-independent budding mechanism controlled by Rab11-FIP2. Proc. Natl. Acad. Sci. U. S. A. **105**:10209–10214.
43. **Berghall H, Wallen C, Hyypia T, Vainionpaa R.** 2004. Role of cytoskeleton components in measles virus replication. Arch. Virol. 149:891–901.

44. Wileman T. 2007. Aggresomes and pericentriolar sites of virus assembly: cellular defense or viral design? Annu. Rev. Microbiol. 61:149–167.
45. Naim HY, Ehler E, Billeter MA. 2000. Measles virus matrix protein specifies apical virus release and glycoprotein sorting in epithelial cells. EMBO J. 19:3576–3585.
46. Riedl P, Moll M, Klenk HD, Maisner A. 2002. Measles virus matrix protein is not cotransported with the viral glycoproteins but requires virus infection for efficient surface targeting. Virus Res. 83:1–12.
47. Jo S, Kawaguchi A, Takizawa N, Morikawa Y, Momose F, Nagata K. 2010. Involvement of vesicular trafficking system in membrane targeting of the progeny influenza virus genome. Microbes Infect. 12:1079–1084.
48. Amorim MJ, Bruce EA, Read EK, Foeglein A, Mahen R, Stuart AD, Digard P. 2011. A Rab11- and microtubule-dependent mechanism for cytoplasmic transport of influenza A virus viral RNA. J. Virol. 85:4143–4156.
49. Duprex WP, McQuaid S, Hangartner L, Billeter MA, Rima BK. 1999. Observation of measles virus cell-to-cell spread in astrocytoma cells by using a green fluorescent protein-expressing recombinant virus. J. Virol. 73:9568–9575.
50. Duprex WP, McQuaid S, Rima BK. 2000. Measles virus-induced disruption of the glial-fibrillary-acidic protein cytoskeleton in an astrocytoma cell line (U-251). J. Virol. 74:3874–3880.
51. Dochow M, Krumm SA, Crowe JE, Jr, Moore ML, Plemper RK. 2012. Independent structural domains in paramyxovirus polymerase protein. J. Biol. Chem. 287:6878–6891.

JVI Journals.ASM.org

Lethal Canine Distemper Virus Outbreak in Cynomolgus Monkeys in Japan in 2008

Kouji Sakai,[a] Noriyo Nagata,[b] Yasushi Ami,[c] Fumio Seki,[a] Yuriko Suzaki,[c] Naoko Iwata-Yoshikawa,[b] Tadaki Suzuki,[b] Shuetsu Fukushi,[d] Tetsuya Mizutani,[d] Tomoki Yoshikawa,[d] Noriyuki Otsuki,[a] Ichiro Kurane,[d] Katsuhiro Komase,[a] Ryoji Yamaguchi,[f] Hideki Hasegawa,[b] Masayuki Saijo,[d] Makoto Takeda,[a] Shigeru Morikawa[d,e]

Department of Virology III,[a] Department of Pathology,[b] Division of Experimental Animal Research,[c] Department of Virology I,[d] Department of Veterinary Science,[e] National Institute of Infectious Diseases, Tokyo, Japan; Department of Veterinary Pathology, Faculty of Agriculture, University of Miyazaki, Miyazaki, Japan[f]

Canine distemper virus (CDV) has recently expanded its host range to nonhuman primates. A large CDV outbreak occurred in rhesus monkeys at a breeding farm in Guangxi Province, China, in 2006, followed by another outbreak in rhesus monkeys at an animal center in Beijing in 2008. In 2008 in Japan, a CDV outbreak also occurred in cynomolgus monkeys imported from China. In that outbreak, 46 monkeys died from severe pneumonia during a quarantine period. A CDV strain (CYN07-dV) was isolated in Vero cells expressing dog signaling lymphocyte activation molecule (SLAM). Phylogenic analysis showed that CYN07-dV was closely related to the recent CDV outbreaks in China, suggesting continuing chains of CDV infection in monkeys. *In vitro*, CYN07-dV uses macaca SLAM and macaca nectin4 as receptors as efficiently as dog SLAM and dog nectin4, respectively. CYN07-dV showed high virulence in experimentally infected cynomolgus monkeys and excreted progeny viruses in oral fluid and feces. These data revealed that some of the CDV strains, like CYN07-dV, have the potential to cause acute systemic infection in monkeys.

Canine distemper virus (CDV) causes acute systemic infection in dogs and other Canidae, with symptoms of fever, coughing, vomiting, diarrhea, ataxia, and paralysis. It has long been thought that only animals in the family Canidae are susceptible to CDV infection in nature. However, during the last 2 decades, animals of many other species, such as Ailuridae (1), Mustelidae (2), Viverridae (3, 4), Procyonidae (5), Phocidae (6), and Felidae (7, 8), have been infected with CDV in nature.

CDV belongs to the genus *Morbillivirus* within the family Paramyxoviridae (9). Signaling lymphocyte activation molecule (SLAM) is a principal receptor of CDV. Other members of the *Morbillivirus* genus, namely, measles virus (MV), rinderpest virus, and peste des petits ruminants virus, are also known to utilize human, bovine, and goat SLAM, respectively, as a receptor. These viruses preferentially use the SLAM of their host animals but have the ability to use other SLAMs of nonhost animals with reduced efficiency (10). Recently, human nectin4 and dog nectin4 have been identified as epithelial cell receptors for MV (11, 12) and CDV (13), respectively.

Importantly, CDV outbreaks have recently emerged with a high mortality rate in nonhuman primates. The first outbreak occurred in 1989 in Japan (14). Twenty-two Japanese monkeys (*Macaca fuscata*) in the wild were captured and later shown to have CDV infections. Two of them developed neurological symptoms, and one died of encephalitis (14). Recently, large CDV outbreaks have occurred in rhesus monkeys (*Macaca mulatta*) at a breeding farm in Guangxi province, China, with a mortality rate of 5 to 30% (15). In 2008, an animal center in Beijing, China, experienced another CDV outbreak in rhesus monkeys (16). This outbreak was likely associated with the Guangxi outbreaks. Following these outbreaks in China, a CDV outbreak occurred in cynomolgus monkeys (*Macaca fascicularis*) in Japan in 2008. These monkeys were imported from China, and some 46 cynomolgus monkeys out of 432 imported were euthanized or died from severe pneumonia, diarrhea, and anorexia during a quarantine period. A CDV strain was isolated from a moribund monkey, and phylogenic analysis of its genome sequence showed that the CDV strain was closely related to the CDV strains associated with recent outbreaks in rhesus monkeys in China, suggesting continuing chains of CDV infection in monkeys. In the present study, we analyzed the pathogenicity of the CDV strain in cynomolgus monkeys. We also investigated whether the CDV strain utilized macaca SLAM and macaca nectin4 as its receptors.

MATERIALS AND METHODS

Cells. Vero cells constitutively expressing dog SLAM (Vero.DogSLAMtag) and dog nectin4 (Vero/dNectin4) were used (13, 17). Vero cells expressing human SLAM (Vero/hSLAM) (10) were also used. Vero cells constitutively expressing macaca SLAM (Vero/macSLAM) and macaca nectin4 (Vero/macNectin4) were generated in the present study. Total RNAs obtained from peripheral blood mononuclear cells (PBMCs) and a kidney from a cynomolgus monkey were used to synthesize cDNAs of macaca SLAM and macaca nectin4, respectively. The nucleotide sequences of cynomolgus SLAM and cynomolgus nectin4 were deposited in GenBank with accession numbers AB742520 and AB742522, respectively. The macaca SLAM and macaca nectin4 cDNA fragments were inserted into the pCXN2 vector (18), generating pCXN2-macSLAM and pCXN2-macNectin4, respectively. Vero/macSLAM and Vero/macNectin4 cells were generated by transfecting Vero cells with pCXN2-macSLAM and pCXN2-macNectin4, respectively, and were selected in Dulbecco's modified Eagle's medium (DMEM) supplemented with 7% fetal bovine serum (FBS) and 0.5 mg/ml Geneticin (G418; Invitrogen). Expression of macaca SLAM and nectin4 in Vero cells was confirmed by immunofluorescence

Received 5 September 2012 **Accepted** 1 November 2012
Published ahead of print 7 November 2012
Address correspondence to Shigeru Morikawa, morikawa@nih.go.jp.

doi:10.1128/JVI.02419-12

staining using a goat anti-human SLAM and nectin4 polyclonal antibody, respectively.

Virus isolation. Tissue samples obtained from the spleens of moribund or dead monkeys were suspended in phosphate-buffered saline (PBS) supplemented with antibiotics and were homogenized. The homogenates were centrifuged at 10,000 × *g* for 5 min, and supernatants were inoculated to monolayers of Vero.DogSLAMtag cells.

RNA extraction and RT-PCR. Viral and total RNAs were extracted from culture media and cells, respectively, using ISOGEN-LS (Nippon Gene). Reverse transcription (RT) was carried out with Superscript III (Invitrogen) using primers of random nucleotide hexamers (TaKaRa Bio Inc.). Then, PCR was performed to amplify CDV-specific cDNA fragments.

Sequencing and phylogenic analysis of the CDV isolate. PCR amplicons were used as templates for sequencing on an Applied Biosystems 3130 automated DNA sequencer using a BigDye Terminator version 3.1 cycle sequencing kit (Applied Biosystems Japan). The entire genome nucleotide sequence was determined using overlapping PCR amplicons. The nucleotide sequence of each extremity was determined by the rapid amplification of cDNA ends (RACE) method. The sequence was further confirmed by using a Roche GS Junior sequencer. Nucleotide and amino acid sequence identities were calculated using the pairwise distance algorithm (*p* distance) with MEGA 4 software (19). Phylograms were reconstructed using a neighbor-joining algorithm with MEGA 4 software. The robustness of the resulting branching patterns was tested using the bootstrap method with 1,000 replicates. Sequence relatedness is shown as percentage identity.

Histopathological examination of monkeys infected with CDV during the 2008 outbreak. Three cynomolgus monkeys (11, 12, and 13) infected with CDV during the 2008 outbreak were euthanized by exsanguination under excess ketamine anesthesia and autopsied for histopathological examination. Tissue samples were immersed in 10% phosphate-buffered formalin. Fixed tissues were embedded in paraffin, sectioned, and stained with hematoxylin and eosin. Immunohistochemical analysis for the detection of the CDV antigens was performed on paraffin-embedded sections using EnVison/HRP Systems (Dako). After deparaffinization with xylene, the sections were rehydrated in ethanol and immersed in PBS. Antigens were retrieved by hydrolytic autoclaving for 15 min at 121°C in a sodium citrate-sodium chloride buffer (10 mM, pH 6.0). Endogenous peroxidase was blocked by incubation in 1% hydrogen peroxide in methanol for 30 min. The sections were incubated with a monoclonal antibody against CDV nucleoprotein (NP) (VMRD Inc.) and then with biotin-conjugated anti-mouse IgG. Peroxidase activity was detected by development with diaminobenzidine containing hydrogen peroxide, and then the nuclei were counterstained by hematoxylin.

Double immunofluorescence stainings were also performed for the various tissues of the CDV-infected cynomolgus monkey 11. Rabbit anti-wide-spectrum cytokeratin antibody (ab9377; Abcam), rabbit anti-neuron-specific β III tubulin antibody (ab56110; Abcam), rabbit anti-CD3 antibody [SP7] (ab21703; Abcam), goat anti-nectin4 polyclonal antibody (R&D Systems), and the monoclonal antibody against CDV NP were used as primary antibodies. Normal rabbit, goat, and mouse sera were used as negative-control antibodies (Dako). The sections were deparaffinized, rehydrated, and immersed in PBS. Antigens were retrieved by hydrolytic autoclaving in the retrieval solution (pH 9.0; Nichirei) for 15 min at 121°C. After the sections were cooled, to block background staining, normal goat or donkey sera were used. The sections were incubated with the monoclonal antibody against CDV NP overnight at 4°C. The sections were washed and incubated with antibodies to the cell markers for 60 min at 37°C. The sections were washed and incubated with goat anti-rabbit IgG-Alexa Fluor 568 (Invitrogen) and goat anti-mouse IgG-Alexa Fluor 488 (Invitrogen) antibodies or donkey anti-goat IgG-Alexa Fluor 568 (Invitrogen) and donkey anti-mouse IgG-Alexa Fluor 488 (Invitrogen) antibodies for 60 min at 37°C. After being washed, the sections were mounted with SlowFade Gold antifade reagent with 4′,6-diamidino-2-phenylindole (DAPI) (Invitrogen). The images were captured by a fluorescence microscopy (IX71; Olympus) equipped with a Hamamatsu high-resolution digital black and white charge-coupled-device (CCD) camera (ORCA2; Hamamatsu Photonics).

Experimental infection of cynomolgus monkeys. Five cynomolgus monkeys of 5 to 11 years of age were obtained from the Tsukuba Primate Research Center (National Institute of Biomedical Innovation, Ibaraki, Japan). They were free from simian retrovirus type 4 (SRV) and were confirmed to be free from MV and CDV antibodies. Four of them (no. 4450, 4571, 4965, 4969) were male, while one (no. 4970) was female. Their cages were placed in negatively pressurized glove boxes. They were anesthetized with ketamine (0.1 ml/kg) and inoculated intranasally with 5×10^5 PFU of CDV in 0.5 ml of DMEM using a spray (0.25 ml in each nostril; Keytron). On the day of inoculation, and at 3, 7, 10, and 15 days after inoculation, body weight and body temperature were measured, and throat and rectal swabs and peripheral blood were obtained. PBMCs were isolated using Percoll gradients (GE Healthcare), adjusted to a concentration of 10^5/ml, and divided into 2-fold serial dilutions. Then, a 500-μl aliquot of each diluted PBMC sample was inoculated into Vero.DogSLAMtag cells. On the assumption that one CDV-infected PBMC was contained in the maximum diluted PBMC sample that induced syncytium, the number of CDV-infected PBMC/10^5 PBMCs was calculated. All monkeys were euthanized 15 days after inoculation by exsanguination under excess ketamine anesthesia, and tissue samples were collected for histopathological examination and virus isolation. For virus isolation, tissue homogenates were prepared in PBS containing antibiotics and clarified by centrifugation. These samples were inoculated to Vero.DogSLAMtag cells. When no cytopathic effect (CPE) was observed, RT-PCR was performed for the detection of CDV-specific RNAs. When no CDV-specific cDNA was amplified, samples were determined as being negative for CDV. Total numbers of blood cells were measured using an autoanalyzer (Cell Tuck; Nihon Koden). Numbers of neutrophils, lymphocytes, monocytes, eosinophils, and basophils were determined by microscopic analysis. A virus-neutralization test for CDV was performed using a plaque reduction method with a constant amount of virus and various serum dilution. Sample sera were serially diluted 4-fold and mixed with equal volumes of 100 PFU of CDV units. The neutralizing antibody titer was calculated at the 50% plaque reduction point by the Behrens-Kaerber method.

Multiplex analysis of cytokines and chemokines in monkey sera. Monkey sera were subjected to multiplex cytokine analysis using the human cytokine 25-plex antibody bead kit (Invitrogen) with Luminex 100 (Luminex Co.) according to the manufacturer's instructions. Enzyme-linked immunosorbent assays (ELISAs) were performed in duplicate, and the averages of each assay are shown.

Replication kinetics of the CDV isolate in Vero cells expressing SLAM and nectin4 of various animal species. Vero, Vero.DogSLAMtag, Vero/macSLAM, Vero/hSLAM, Vero/dNectin4, and Vero/macNectin4 cells (2×10^5 cells/well) were cultured in 24-well plates and infected with the CDV isolate at a multiplicity of infection (MOI) of 0.01. The cells were adsorbed with the virus for 1 h at 37°C, and then the virus inoculum was removed and the cells were rinsed twice with DMEM. The cells were cultured in DMEM supplemented with 1% fetal calf serum (FCS) at 37°C. The cells and culture supernatants were harvested every 12 h until 3 days postinfection (p.i.). The harvested samples were stored at −80°C until use. The samples were centrifuged at 1,000 × *g* and titrated with plaque assay.

Cell-to-cell fusion assay. DNA fragments encoding H and F protein of the CDV isolate were amplified by RT-PCR and cloned into the pCAGGS vector (18). Vero, Vero.DogSLAMtag, Vero/macSLAM, Vero/hSLAM, Vero/dNectin4, Vero/macNectin4, and Vero cells in 24-well plates were transfected with the F protein-expressing plasmid together with or without the H protein-expressing plasmid. To detect syncytia clearly, a fluorescent protein-expressing plasmid, pEGFP-C1 (Clontech Laboratories),

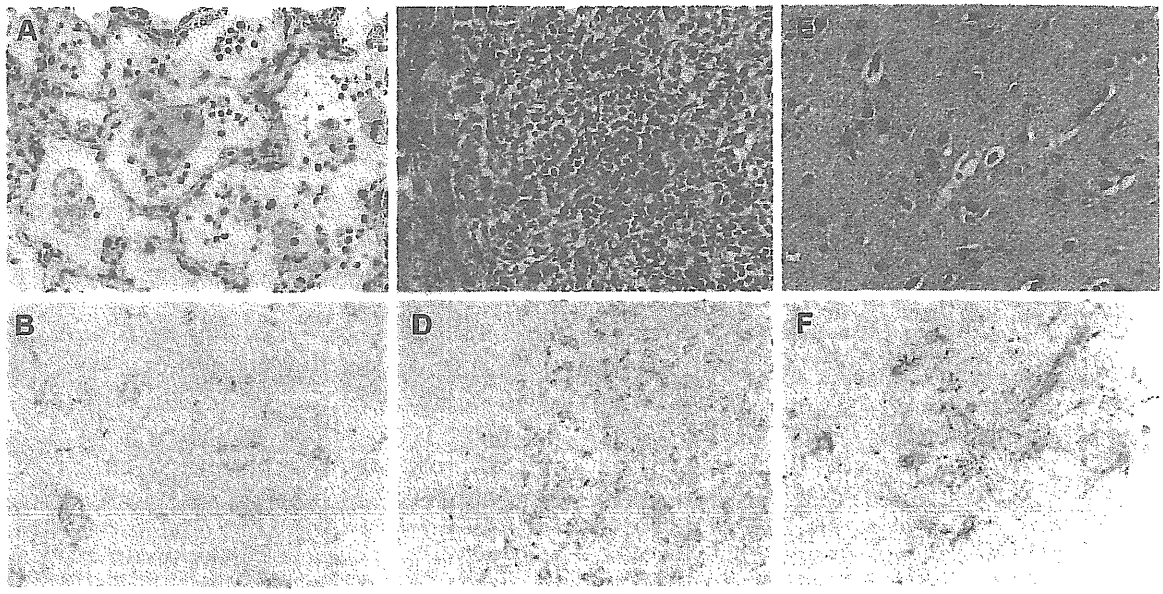

FIG 1 Histopathological analyses of cynomolgus monkeys naturally infected with CDV in the 2008 outbreak. Tissue sections obtained from cynomolgus monkey 11 were examined by hematoxylin and eosin staining (HE) and immunohistochemistry (IHC) using anti-CDV-NP monoclonal antibody. Giant cell pneumonia (A) and CDV antigen in the syncytial pneumocytes (B) were seen in the lung. Lymphocyte depletion (C) and CDV antigen in the mononuclear cells (D) were observed in the lymph node. Focal and slight microglia cell infiltration (E) and CDV antigen in neurons and glia cells (F) were observed in the cerebrum. HE, original magnification ×20; IHC, ×40.

was cotransfected. The cell monolayers were observed using an Axio Observer.D1 microscope at 16 and 24 h posttransfection.

Entry assay using pseudotyped viruses. To analyze the efficiency of virus entry using SLAM and nectin4 in more detail, a vesicular stomatitis virus (VSV) pseudotype system (17) was employed (VSVΔG* was kindly provided by M. A. Whitt, The University of Tennessee Health Science Center). A VSV pseudotype bearing the H protein and the F protein of the CDV strain on the surface of the virion (referred to as VSVΔG*-F-dVH) was constructed. VSV pseudotype bearing only the F protein (referred to as VSVΔG*-F) was also constructed. Vero, Vero.DogSLAMtag, Vero/macSLAM, Vero/dNectin4, and Vero/macNectin4 cells were infected with the VSV pseudotypes. Infectivity titers of the VSVΔG*-F-dVH and VSVΔG*-F were determined at 24 h p.i.

Ethics statement. The experiments with animals were performed at animal biological safety level 2 in strict accordance with the Animal Experimentation Guidelines of the National Institute of Infectious Diseases. The protocol was approved by the Institutional Animal Care and Use Committee of the institute (permit number 611001). Collection of the specimens from the monkeys was performed under ketamine hydrochloride anesthesia, and all efforts were made to minimize suffering.

RESULTS

Clinical and pathological features of cynomolgus monkeys naturally infected with CDV in the outbreak in Japan. Forty-six monkeys out of 432 cynomolgus monkeys died or were euthanized during a quarantine period after import from China in Japan in 2008, resulting in a fatality rate of 10.6% (46/432) if euthanized animals were considered to be fatal. Clinical signs of sick monkeys were characterized by eye mucus, nasal mucus, rhinitis, coughing, anorexia, diarrhea, fever, and generalized rash, which are similar to those observed in acute measles in humans and in monkeys in recent CDV outbreaks in China. Swelling of the footpads was also observed in sick monkeys. Three moribund monkeys were autopsied for histopathological examination. Histopathologically, two monkeys (animals 11 and 12) were in the acute phase of systemic CDV infection. One monkey (animal 13) was considered to be in a convalescent phase. Various stages of giant cell pneumonia were found in all three monkeys (Fig. 1A). CDV antigen-positive syncytial pneumocytes were seen in the lungs of two monkeys (animals 11 and 12) (Fig. 1B). In the thymus, spleen, tonsils, and lymph nodes of all monkeys, almost all lymphocytes were depleted, suggesting severe immune suppression. The remaining mononuclear cells were positive for CDV antigen in the lymph tissues of two monkeys (animals 11 and 12) (Fig. 1C and D). Focal gliosis and demyelination were found in the cerebrum and/or cerebellum of all monkeys. In these lesions, some neurons and glia cells were positive for CDV antigen in all monkeys (Fig. 1E and F). In other organs, including the skin, small and large intestines, kidneys, salivary glands, and testes, giant cells and/or CDV antigen-positive cells were observed. Interestingly, CDV antigen-positive cells were not observed in the tissues except for the brain and testis of monkey 13. The types of cells with CDV antigens in the tissues were identified by dual staining with antibodies to CDV NP and various cell markers (Fig. 2). CDV antigens were detected in some of the cytokeratin-positive giant cells in the bronchi and bronchiole (Fig. 2). The bronchiolar epithelial cells with CDV antigens were also necitin4 positive (Fig. 2). In addition, the virus antigens were also detected in the $CD3^+$ lymphocytes in the lymph node and the βIII tubulin-positive neurons in the brain (Fig. 2). Sera of the three monkeys (no. 11, 12, and 13) were subjected to multiplex cytokine analysis. Compared with eight normal monkeys from Tsukuba Primate Research Center, naturally CDV-infected monkeys in the outbreak showed upregulated levels of proinflammatory cytokines and chemokines, such as interleukin 1β (IL-1β), IL-6, macrophage inflammatory protein 1α (MIP-1α), MIP-1β, monocyte chemoattractant protein 1

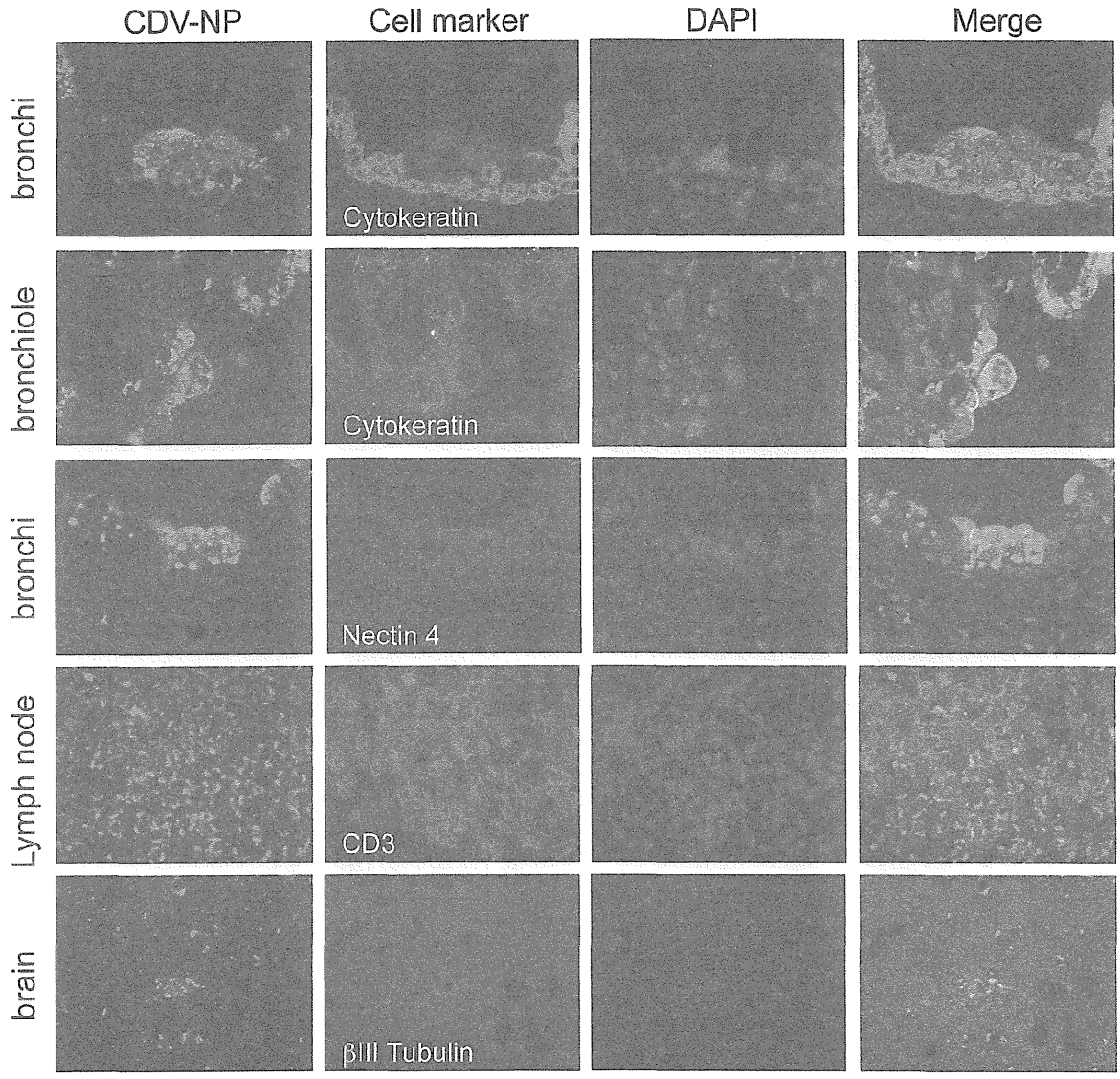

FIG 2 Double immunofluorescence staining of tissues of cynomolgus monkey 11 naturally infected with CDV in the 2008 outbreak. Tissue sections obtained from cynomolgus monkey 11 were examined by double immunofluorescence staining with anti-CDV-NP antibody and rabbit anti-cytokeratin, rabbit anti-neuron-specific β III tubulin, rabbit anti-CD3, or goat anti-nectin4 antibody. CDV-NP antigens were detected in the bronchi, bronchiole, lymph node, and brain. Some CDV-NP antigen-positive cells were positive for cytokeratin, nectin4, or CD3. A few CDV-NP antigen-positive neurons were positive for βIII tubulin.

(MCP-1), and eotaxin. Proinflammatory cytokines associated with T cell activation, gamma interferon (IFN-γ) and IL-15, were also found. Anti-inflammatory responses of IL-1 receptor antagonist (IL-1ra) were also upregulated in the monkeys (Table 1).

Isolation of CDV from monkeys using Vero.DogSLAMtag cells. Typical syncytia developed in monolayers of Vero.DogSLAMtag cells at as early as 2 days p.i. of spleen homogenates obtained from dead or moribund monkeys. However, syncytia were not observed in Vero cells inoculated with the spleen homogenates (data not shown). One of the CDV isolates was named CYN07-dV.

Relationship between CYN07-dV and Chinese CDV strains associated with monkey outbreaks. The entire genome nucleo-

TABLE 1 Blood chemokine/cytokine levels

Cytokine	Monkeys naturally infected with CDV			Normal monkeys			*P* value[a]
	Median (pg/ml)	SD	No. positive/ no. tested	Median (pg/ml)	SD	No. positive/ no. tested	
IL-1β	120	66	2/3	<17		0/8	0.023*
IL-6	94	72	3/3	<9		0/8	0.011*
MIP-1α	228	78	3/3	84	48	8/8	0.000**
MIP-1β	157	61	3/3	40	36	7/8	0.001**
MCP-1	3,917	2,286	3/3	461	245	8/8	0.043*
Eotaxin	2,121	1,096	3/3	413	203	8/8	0.023*
IFN-γ	509	150	3/3	261	183	3/8	0.002*
IL-15	89	65	2/3	64	23	1/8	0.115

[a] Asterisks indicate statistically significant differences between monkeys naturally infected with CDV and normal monkeys (*, $P < 0.05$; **, $P < 0.001$).

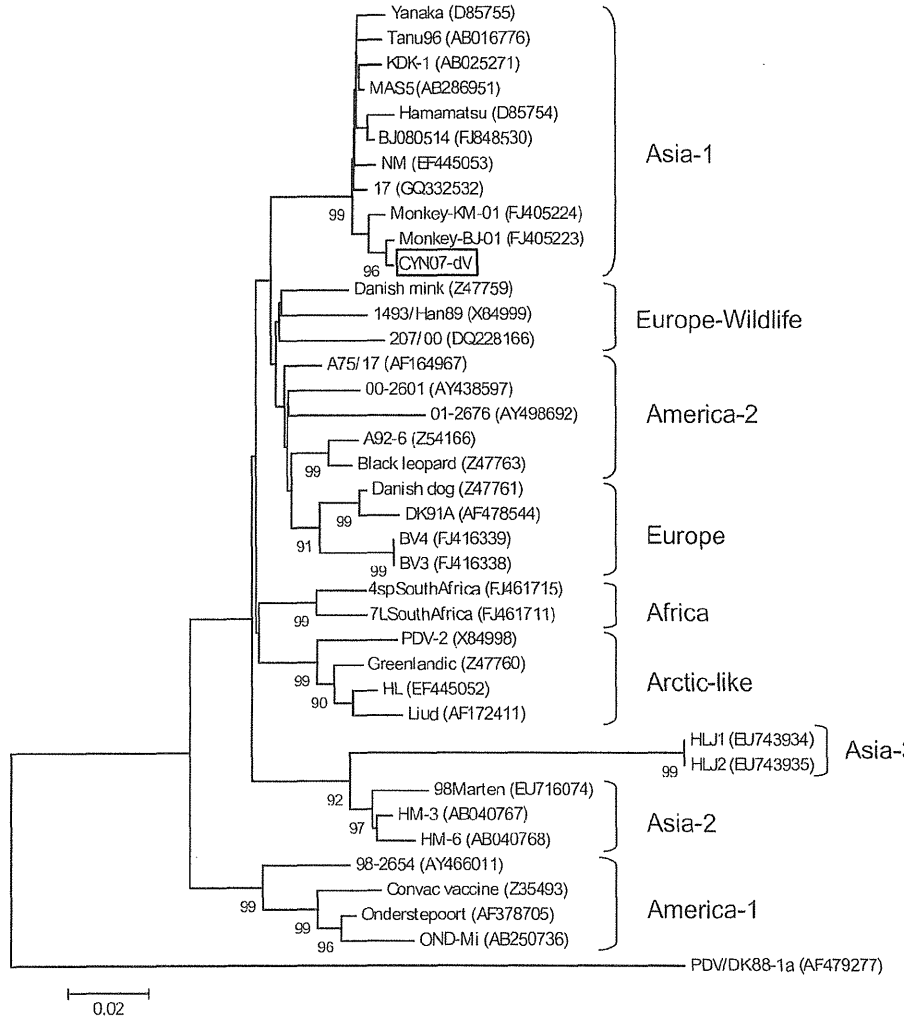

FIG 3 Phylogenetic tree of CDV based on the CYN07-dV sequence. Phylogenetic analysis of the H protein of the CDV showed that the CYN07-dV was closely related to the CDV strains isolated from rhesus monkeys in China. Scale bars indicate phylogenetic distance between CDV isolates.

tide sequence of the CDV strain CYN07-dV was determined (DDBJ/GenBank accession number AB687720). A phylogenic analysis of H protein indicated that CYN07-dV belongs to the Asia-1 clade and is closely related to monkey-BJ-01 and monkey-KM-01 strains (GenBank accession numbers FJ405223 and FJ405224, respectively) isolated from rhesus monkeys in China in 2008 (15) (Fig. 3). Comparative analyses throughout the genomes of CDV strains revealed that CYN07-dV showed the highest homology to the monkey-KM08 strain isolated from a rhesus monkey in China in 2008 (GenBank accession number HM852904) (15) (99.6%; 15,632/15,690 nucleotides). A phylogenic analysis indicated that CYN07-dV showed high homology with CDV isolates from different animal species in China (NM strain isolated from foxes in China and 17 strains isolated from dogs in China), suggesting a Chinese source of the CYN07-dV strain.

Experimental infection of cynomolgus monkeys with CYN07-dV. Five cynomolgus monkeys were infected intranasally with CYN07-dV. In these animals, no lethal infection was observed during an experimental period of 15 days, and clinical symptoms were less severe than those observed in the moribund and dead monkeys during the outbreak. However, all five monkeys had appetite loss at 7 to 12 days p.i. Body weight was decreased in three of the five monkeys (Fig. 4A). The rectal temperature was transiently increased at 3 to 7 days p.i. in some monkeys (Fig. 4B). In all five monkeys, the numbers of white blood cells and lymphocytes were decreased (Fig. 4C and D), as the numbers of CDV-infected PBMCs were increased (Fig. 4E). Neutralizing antibodies against CDV were detected in the monkey sera at 7 days p.i., and then the titers of antibodies were raised at 10 days p.i. (Fig. 4F). Infectious CDV was isolated from various tissues of autopsied specimens at 15 days p.i., including local lymph nodes, lungs, liver, kidneys, intestinal tracts, and central nervous tissues of monkeys (Table 2, 3). In monkey 4965, giant cells were observed in the alveolar area of the lungs where the syncytial pneumocytes were positive for CDV antigen (Fig. 5A and B), and lymphocytes were depleted in the lymph nodes where the follicular cells and mononuclear cells were positive for CDV antigen (Fig. 5C and D). These histopathological findings were also observed in

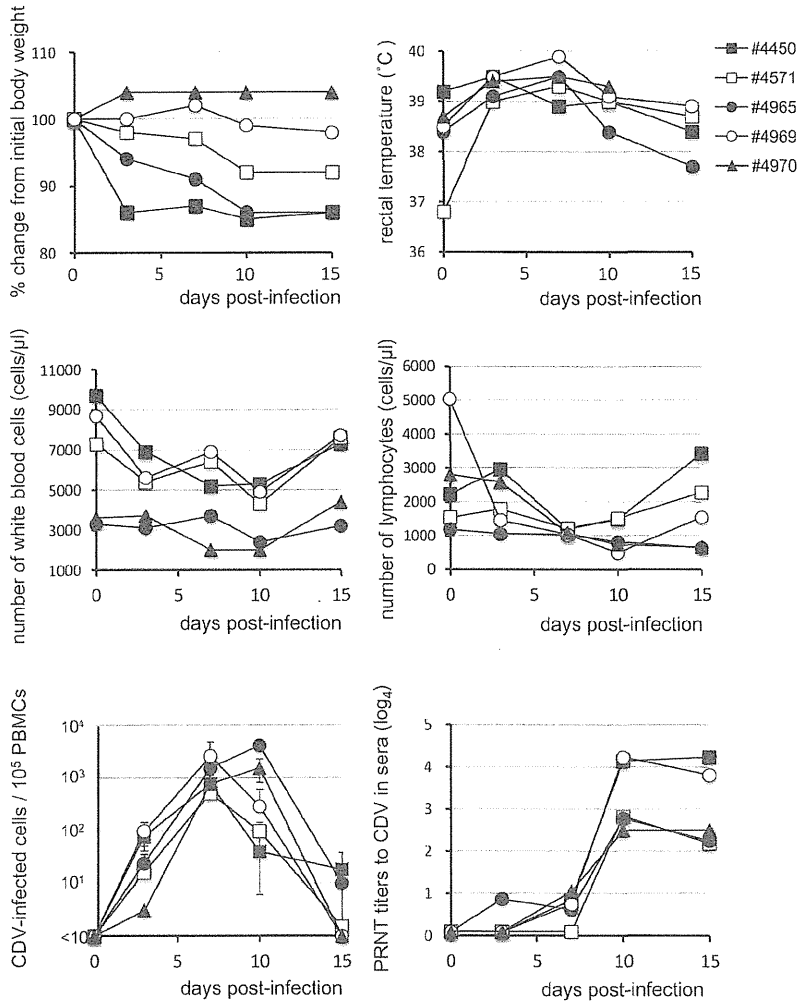

FIG 4 Changes in body weight, rectal temperature, and the numbers of white blood cells, lymphocytes, and CDV-infected PBMCs and neutralization antibody level in the experimentally CDV-infected monkeys. (A) Body weight; (B) rectal temperature; (C) white blood cell count; (D) lymphocytes count; (E) CDV-infected PBMC count; (F) neutralizing antibodies against CDV.

other monkeys but were less severe than those in monkey 4965 (data not shown). The experimentally CDV-infected monkeys showed upregulated levels of IFN-α and IL-1ra at 7 to 10 days p.i. Some monkeys showed upregulated levels of MIP-1β, MCP-1, eotaxin, IFN-γ, and IL-15 (data not shown).

The nucleotide and amino acid sequences of SLAM and nectin4 of cynomolgus monkeys. The nucleotide and deduced amino acid sequences of SLAM and nectin4 of cynomolgus monkeys were determined (DDBJ/GenBank accession numbers AB742520 and AB742522, respectively). Cynomolgus monkey

TABLE 2 CDV isolation from various organs in the experimentally infected cynomolgus monkeys at 15 days p.i.

	Result[a]									
Animal no.	Skin	Respiratory	Liver	Kidney	Intestine	Spleen	Lymph node[b]	Thymus	Tonsil	Central nervous system
4450	−	+	−	−	+	−	−	−	−	−
4571	−	+	−	−	+	+	+	+	+	−
4965	−	+	+	+	+	+	+	+	+	+
4969	−	−	−	−	−	−	−	−	−	−
4970	−	+	−	−	−	−	−	+	+	−

[a] −, CDV negative; +, CDV positive.
[b] Cervical and intestinal lymph node.

TABLE 3 CDV isolation from throat swabs, rectal swabs, and feces in the experimentally infected cynomolgus monkeys

	Result by day p.i.[a]																
	Throat swabs					Rectal swabs					Feces						
Animal no.	0	3	7	10	15	0	3	7	10	15	1–9	10	11	12	13	14	15
4450	−	−	−	−	−	−	−	+	+	−	−	−	+	+	−	−	−
4571	−	−	−	+	−	−	−	−	+	−	−	+	+	+	+	+	+
4965	−	−	−	+	+	−	−	−	+	−	−	+	+	−	+	+	+
4969	−	−	−	−	−	−	−	−	+	−	−	−	+	+	−	−	−
4970	−	−	−	−	−	−	−	−	−	−	−	−	−	−	−	−	−

[a] −, CDV negative; +, CDV positive.

SLAM showed high levels of identity to rhesus monkey SLAM (DDBJ/EMBL/GenBank accession no. XM_001117605) and human SLAM (DDBJ/EMBL/GenBank accession no. U33017), with 99.9% (100%) and 97.6% (96.7%) nucleotide (amino acid) identity, respectively. Amino acid sequences of the SLAM were completely conserved among three macaques: cynomolgus monkey, rhesus monkey, and pig-tailed monkey (AB742521) (data not shown). On the other hand, cynomolgus monkey SLAM showed a lower level of identity to dog SLAM (DDBJ/EMBL/GenBank accession no. AF390108), with 76.5% (65.0%) nucleotide (amino acid) identity.

Cynomolgus monkey nectin4 showed identity to dog nectin4 (DDBJ/EMBL/GenBank accession no. AB755429), rhesus monkey nectin4 (DDBJ/EMBL/GenBank accession no. XM_001117709), and human nectin4 (DDBJ/EMBL/GenBank accession no. NM_030916), with 89.0% (94.1%), 100% (100%), and 98.3% (99.4%) nucleotide (amino acid) identity, respectively.

CDV strain CYN07-dV utilizes macaca SLAM and macaca nectin4 as receptors. The replication kinetics of CYN07-dV was analyzed in Vero, Vero.DogSLAMtag, Vero/macSLAM, Vero/hSLAM, Vero/dNectin4, and Vero/macNectin4 cells. In Vero and Vero/hSLAM cells, CYN07-dV replicated inefficiently (Fig. 6A). On the other hand, it replicated efficiently in Vero.DogSLAMtag, Vero/macSLAM, Vero/dNectin4, and Vero/macNectin4 cells. The peak titer and replication kinetics of the virus in Vero/macSLAM cells were comparable to those in Vero.DogSLAMtag cells (Fig. 6A). The peak titer of the virus in Vero/macNectin4 cells was also comparable to that in Vero/dNectin4, although virus production was slightly delayed in Vero/macNectin4 cells (Fig. 6A). The wild-type CDV strain Ac96I (13), isolated from

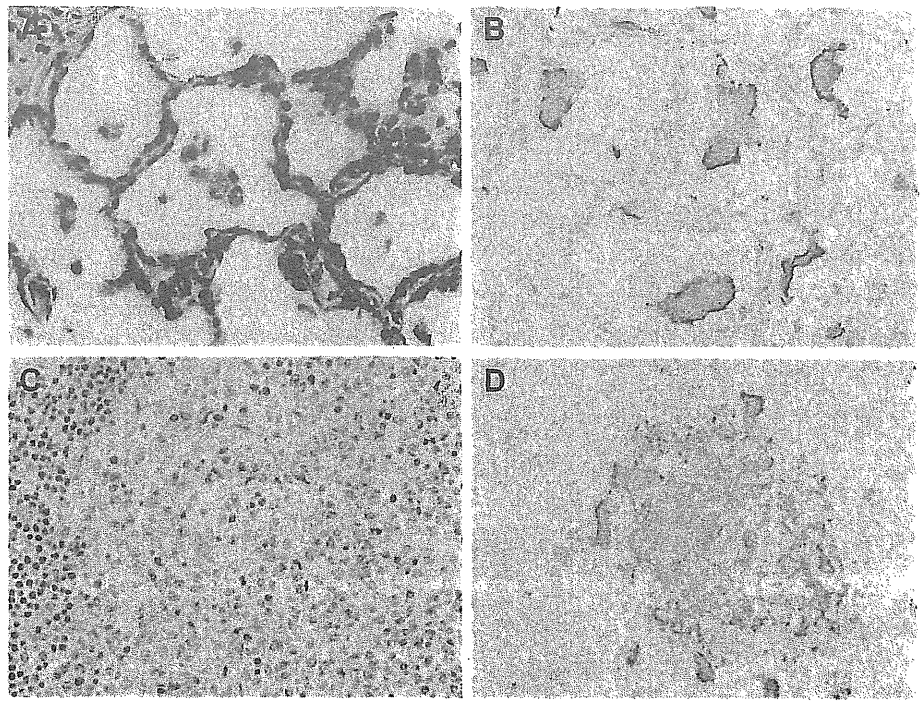

FIG 5 Histopathological analyses of cynomolgus monkeys experimentally infected with CDV. Tissue sections obtained from cynomolgus monkey 4965 were examined by hematoxylin and eosin staining and immunohistochemistry using anti-CDV-NP monoclonal antibody. Giant cells (A) with CDV antigen (B) were observed in the alveolar area in the lung. Lymphocyte depletion (C) and CDV antigen-positive cells were observed in the follicular area (D) in the lymph node of CYN07-dV-infected monkey 4965. HE, ×20; IHC, ×40.

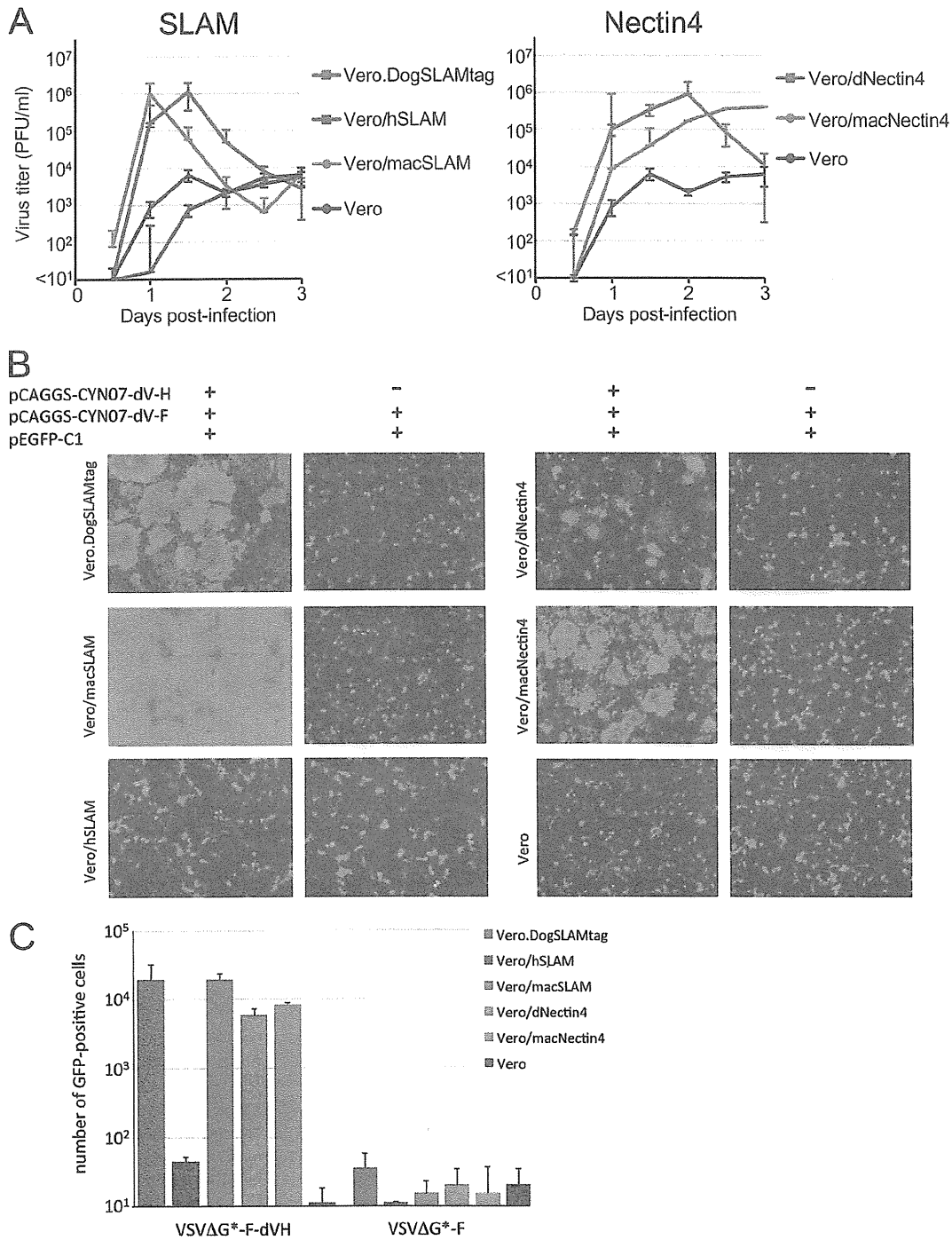

FIG 6 CYN07-dV utilizes macaca SLAM and macaca nectin4 as receptors. (A) Growth kinetics of CYN07-dV in Vero.DogSLAMtag, Vero/hSLAM, Vero/macSLAM, Vero/dNectin4, Vero/macNectin4, and Vero cells. The cells were infected with the virus at an MOI of 0.01, and titers at the indicated points were shown. (B) Induction of syncytium upon transfection with a mixture of plasmids expressing enhanced green fluorescent protein (EGFP) and CDV F with or without a plasmid expressing CDV H. (C) Infectivity of VSV pseudotype bearing H and F proteins of CYN07-dV (VSVΔG*-F-dVH) or that bearing the F protein (VSVΔG*-F) in Vero.DogSLAMtag, Vero/hSLAM, Vero/macSLAM, Vero/dNectin4, Vero/macNectin4, and Vero cells.

a sick dog, also replicated in the Vero/macSLAM cells; however, the appearance of synsytia was delayed in the Vero/macSLAM cells compared with that in the Vero.DogSLAMtag cells, and the peak titer of the virus in the Vero/macSLAM cells was significantly lower than that in the Vero.DogSLAMtag cells (data not shown).

To clarify whether the H and the F proteins of the virus induce syncytia in the cells expressing either SLAM or nectin4, cell-to-cell

fusion assay was performed upon transfection of the plasmids expressing the F and the H proteins of CYN07-dV. No syncytium formation was detected when the F protein of CYN07-dV alone was expressed in the cells (data not shown). On the other hand, many syncytia were observed in Vero.DogSLAMtag, Vero/macSLAM, Vero/dNectin4, and Vero/macNectin4 cells, but not in Vero and Vero/hSLAM cells, when the F and the H protein of CYN07-dV were expressed together (Fig. 6B). The syncytium formation was most remarkable in Vero/macSLAM cells (Fig. 6B). Although syncytia in nectin4-expressing Vero cells (Vero/dNectin4 and Vero/macNectin4) were smaller than those in SLAM-expressing cells (Vero.DogSLAMtag and Vero/macSLAM), syncytia in Vero/macNectin4 and Vero/dNectin4 cells were comparable (Fig. 6B).

To clarify the function of the H and the F proteins on entry of the virus via the SLAM and the nectin4, the infectivities of the VSV pseudotype bearing the H and the F protein of CYN07-dV, VSVΔG*-F-dVH, in various cells were compared. The VSV pseudotype bearing the F protein alone, VSVΔG*-F, did not infect any cells tested, whereas the VSVΔG*-F-dVH efficiently infected Vero/macSLAM cells and Vero.DogSLAMtag cells (Fig. 6C) but did not infect Vero/hSLAM cells. The VSVΔG*-F-dVH also efficiently infected Vero/macNectin4 cells and Vero/dNectin4 cells (Fig. 6C). These data showed that the CYN07-dV H protein efficiently utilizes macaca SLAM and macaca nectin4 as receptors.

DISCUSSION

Viruses in the genus *Morbillivirus* often cause severe diseases in animals and humans. Generally, symptomatic infection with each morbillivirus occurs in specific animal species or humans. Among the morbilliviruses, MV is the one that causes an acute febrile and systemic infection in humans. Although CDV also shows host specificity and causes acute infections primarily in dogs, it often affects animals in different species, including nonhuman primates, showing a high mortality rate. In the CDV outbreak that occurred among Japanese monkeys in Japan in 1989, only one monkey out of 34 died (14). However, in recent outbreaks in China and Japan, higher mortality rates were recorded: 4,250 monkeys out of ~10,000 died in Guangxi Province in 2006, 12 out of 20 died in Beijing in 2008, and 46 out of 432 died in Japan in 2008. Most authorized animal suppliers in China receive monkeys from a Guangxi farm and distribute monkeys to researchers throughout the mainland of China. Laboratory investigations of clinical specimens from moribund and/or dead monkeys in the present study and in earlier studies (15, 16) fulfilled the two criteria of Koch's postulates: (i) detection of CDV in sick animals and (ii) isolation of CDV in cultured cells. The experimental infection in the study further fulfill the remaining postulates: (iii) induction of a comparable disease in the original host and (iv) reisolation of CDV from experimentally infected animals. These findings proved that CDV is the primary cause of the outbreak in monkeys. Moreover, the numbers of monkeys infected with CDV in the Guangxi farm decreased greatly after the introduction of attenuated CDV vaccination in early 2009, even though a few cases have still been reported every year (15).

In the present study, mortality was not observed in experimentally CDV-infected monkeys. However, many monkeys, especially those that eventually became CDV antibody-positive at the outbreak, showed mild or no symptoms. Severe symptoms were observed only in some moribund and dead monkeys in the outbreak. Thus, mortality might have been observed if more monkeys were experimentally infected, even though we could not rule out the possibility of enhanced pathogenicity of CDV by coinfection of some other agent during the outbreak. To date, no other particular agents were detected in the monkeys. However, we could not rule out the possibility that isolation and passage of the virus in Vero/dog.SLAM could have caused a partial attenuation of the virus. This may be clarified in future to analyze the quasispecies of genome sequences of the virus in the original clinical samples of the monkey and to compare them to the sequence of the isolated virus.

In the present study, three moribund monkeys in the 2008 CDV outbreak showed upregulated levels of proinflammatory cytokines and chemokines, such as IL-1β, IL-6, MIP-1α, MIP-1β, MCP-1, eotaxin, IFN-γ, and IL-15. Anti-inflammatory responses of IL-1ra were also upregulated. In the rhesus monkeys infected with measles virus, suppression of IL-12 in the sera was reported (20). The induction of IFN-γ, IL-2, and MCP-1 in the sera of the measles virus-infected cynomolgus monkeys was also reported (21). However, comparable levels of upregulation in proinflammatory cytokines, chemokines, and anti-inflammatory responses of IL-1 receptor antagonist observed in the CDV-infected monkeys were not reported for the measles virus-infected monkeys. These observations are rather similar to rhesus monkeys infected with a lethal dose of Zaire ebolavirus (22). The mixed anti-inflammatory response syndrome in Zaire ebolavirus-infected monkeys is characterized by highly elevated levels of IL-13 and IL-1ra, which are similar to the CDV-infected monkeys in the outbreak. Thus, unbalanced responses of cytokines and chemokines may have contributed to the pathogenesis of fatal cases of CDV infection in monkeys in the outbreak.

The CYN07-dV efficiently infected Vero cells expressing dog and macaca SLAM but not the cells expressing human SLAM. This was confirmed by syncytium induction upon transient expression of the H and the F proteins of the virus and also by infectivity of the VSV pseudotype bearing the H and the F proteins of the virus. On the other hand, the CYN07-dV efficiently utilized nectin4 of dog and macaca. Thus, the CYN07-dV is capable of utilizing macaca SLAM and macaca nectin4 as receptors, as efficiently as dog SLAM and dog nectin4, respectively. These findings were consistent with the experimental infection of the CYN07-dV to cynomolgus monkeys, in which the virus infected PBMCs and epithelial cells expressing macaca SLAM and nectin4, respectively. Interestingly, the CYN07-dV did not efficiently utilize human SLAM as a receptor even though the SLAMs of human and macaca are highly conserved. Thus, at the moment, CDVs like CYN07-dV may not be a direct threat to humans. However, the expansion of host animal species of CDV to include primates might be a global threat in the future. Wild-type CDV strains isolated from dogs with distemper were recently shown to efficiently utilize both dog SLAM and dog nectin4 as receptors (13, 17). However, the wild-type CDV strain Ac96I also replicated in the Vero/macSLAM cells even though less efficiently than in the Vero.DogSLAMtag cells. This suggested that some wild-type CDV strain is capable of utilizing macaca SLAM as a receptor *per se*, even though the CYN07-dV utilizes macaca SLAM more efficiently. Thus, the CYN07-dV is considered to be adapted to spread among monkeys using macaca SLAM and macaca nectin4.

Nucleotide and amino acid sequence accession numbers. The complete nucleotide sequence of the CYN07-dV has been

deposited in DDBJ/GenBank under accession number AB687720, while the amino acid sequence of hemagglutinin protein has been deposited in DDBJ/GenBank under accession number BAM15593. The complete nucleotide sequences of mRNAs of cynomolgus monkey SLAM, pig-tailed monkey SLAM, and cynomolgus monkey nectin4 have been deposited in DDBJ/GenBank under accession numbers AB742520, AB742521, and AB742522, respectively.

ACKNOWLEDGMENTS

We thank Yusuke Yanagi for providing Vero.DogSLAMtag and Vero/hSLAM cells.

This work was supported in part by grants-in-aid from the Ministry of Health, Labor, and Welfare of Japan (grants H22-shinkou-ippan-006 and H24-kokui-shitei-003) and KAKENHI [Grant-in-Aid for Young Scientists (B), 22700459] from the Japan Society for the Promotion of Science (http://www.jsps.go.jp/english/).

REFERENCES

1. Kotani T, Jyo M, Odagiri Y, Sakakibara Y, Horiuchi T. 1989. Canine distemper virus infection in lesser pandas (*Ailurus fulgens*). Nihon Juigaku Zasshi. 51:1263–1266.
2. Perpiñán D, Ramis A, Tomás A, Carpintero E, Bargalló F. 2008. Outbreak of canine distemper in domestic ferrets (*Mustela putorius furo*). Vet. Rec. 163:246–250.
3. Hirama K, Goto Y, Uema M, Endo Y, Miura R, Kai C. 2004. Phylogenetic analysis of the hemagglutinin (H) gene of canine distemper viruses isolated from wild masked palm civets (*Paguma larvata*). J. Vet. Med. Sci. 66:1575–1578.
4. Hur K, Bae JS, Choi JH, Kim JH, Kwon SW, Lee KW, Kim DY. 1999. Canine distemper virus infection in binturongs (*Arctictis binturong*). J. Comp. Pathol. 121:295–299.
5. Roscoe DE. 1993. Epizootiology of canine distemper in New Jersey raccoons. J. Wildl. Dis. 29:390–395.
6. Osterhaus AD, Groen J, De Vries P, UytdeHaag FG, Klingeborn B, Zarnke R. 1988. Canine distemper virus in seals. Nature 335:403–404.
7. Appel MJ, Yates RA, Foley GL, Bernstein JJ, Santinelli S, Spelman LH, Miller LD, Arp LH, Anderson M, Barr M, Pearce-Kelling S, Summers BA. 1994. Canine distemper epizootic in lions, tigers, and leopards in North America. J. Vet. Diagn. Invest. 6:277–288.
8. Roelke-Parker ME, Munson L, Packer C, Kock R, Cleaveland S, Carpenter M, O'Brien SJ, Pospischil A, Hofmann-Lehmann R, Lutz H, Mwamengele GL, Mgasa MN, Machange GA, Summers BA, Appel MJ. 1996. A canine distemper virus epidemic in Serengeti lions (*Panthera leo*). Nature 379:441–445.
9. Robert AL, Griffith DP. 2007. Paramyxoviridae, p 1449–1496. *In* Fields BN, Knipe DM, Howley PM, Griffin DE, Lamb RA, Martin MA, Roizman B, Straus SE (ed), Fields virology, fifth ed. Lippincott-Raven, Philadelphia, PA.
10. Tatsuo H, Ono N, Yanagi Y. 2001. Morbilliviruses use signaling lymphocyte activation molecules (CD150) as cellular receptors. J. Virol. 75:5842–5850.
11. Mühlebach MD, Mateo M, Sinn PL, Prüfer S, Uhlig KM, Leonard VH, Navaratnarajah CK, Frenzke M, Wong XX, Sawatsky B, Ramachandran S, McCray PB, Jr, Cichutek K, von Messling V, Lopez M, Cattaneo R. 2011. Adherens junction protein nectin-4 is the epithelial receptor for measles virus. Nature 480:530–533.
12. Noyce RS, Bondre DG, Ha MN, Lin LT, Sisson G, Tsao MS, Richardson CD. 2011. Tumor cell marker PVRL4 (nectin 4) is an epithelial cell receptor for measles virus. PLoS Pathog. 7:e1002240. doi:10.1371/journal.ppat.1002240.
13. Pratakpiriya W, Seki F, Otsuki N, Sakai K, Fukuhara H, Katamoto H, Hirai T, Maenaka K, Techangamsuwan S, Lan NT, Takeda M, Yamaguchi R. 2012. Nectin4 is an epithelial cell receptor for canine distemper virus and involved in the neurovirulence. J. Virol. 86:10207–10210.
14. Yoshikawa Y, Ochikubo F, Matsubara Y, Tsuruoka H, Ishii M, Shirota K, Nomura Y, Sugiyama M, Yamanouchi K. 1989. Natural infection with canine distemper virus in a Japanese monkey (*Macaca fuscata*). Vet. Microbiol. 20:193–205.
15. Qiu W, Zheng Y, Zhang S, Fan Q, Liu H, Zhang F, Wang W, Liao G, Hu R. 2011. Canine distemper outbreak in rhesus monkeys, China. Emerg. Infect. Dis. 17:1541–1543.
16. Sun Z, Li A, Ye H, Shi Y, Hu Z, Zeng L. 2010. Natural infection with canine distemper virus in hand-feeding Rhesus monkeys in China. Vet. Microbiol. 141:374–378.
17. Seki F, Ono N, Yamaguchi R, Yanagi Y. 2003. Efficient isolation of wild strains of canine distemper virus in Vero cells expressing canine SLAM (CD150) and their adaptability to marmoset B95a cells. J. Virol. 77:9943–9950.
18. Niwa H, Yamamura K, Miyazaki J. 1991. Efficient selection for high-expression transfectants with a novel eukaryotic vector. Gene 108:193–199.
19. Tamura K, Dudley J, Nei M, Kumar S. 2007. MEGA4: molecular evolutionary genetics analysis (MEGA) software version 4.0. Mol. Biol. Evol. 24:1596–1599.
20. Griffin DE, Ward BJ, Jauregui E, Johnson RT, Vaisberg A. 1990. Immune activation during measles: interferon-gamma and neopterin in plasma and cerebrospinal fluid in complicated and uncomplicated disease. J. Infect. Dis. 161:449–453.
21. Takeuchi K, Nagata N, Kato SI, Ami Y, Suzaki Y, Suzuki T, Sato Y, Tsunetsugu-Yokota Y, Mori K, Van Nguyen N, Kimura H, Nagata K. 2012. Wild-type measles virus with the hemagglutinin protein of the Edmonston vaccine strain retains wild-type tropism in macaques. J. Virol. 86:3027–3037.
22. Ebihara H, Rockx B, Marzi A, Feldmann F, Haddock E, Brining D, LaCasse RA, Gardner D, Feldmann H. 2011. Host response dynamics following lethal infection of rhesus macaques with Zaire ebolavirus. J. Infect. Dis. 204(Suppl 3):S991–S999.

Virology 435 (2013) 485–492

Contents lists available at SciVerse ScienceDirect

Virology

journal homepage: www.elsevier.com/locate/yviro

Canine distemper virus with the intact C protein has the potential to replicate in human epithelial cells by using human nectin4 as a receptor

Noriyuki Otsuki [a,*], Tsuyoshi Sekizuka [b], Fumio Seki [a], Kouji Sakai [a], Toru Kubota [a], Yuichiro Nakatsu [a], Surui Chen [c], Hideo Fukuhara [c], Katsumi Maenaka [c], Ryoji Yamaguchi [d], Makoto Kuroda [b], Makoto Takeda [a]

[a] Department of Virology 3, National Institute of Infectious Diseases, Gakuen 4-7-1, Musashimurayama, Tokyo 208-0011, Japan
[b] Laboratory of Bacterial Genomics, Pathogen Genomics Center, National Institute of Infectious Diseases, Tokyo, Japan
[c] Laboratory of Biomolecular Science, Faculty of Pharmaceutical Sciences, Hokkaido University, Sapporo, Japan
[d] Department of Veterinary Pathology, Faculty of Agriculture, University of Miyazaki, Miyazaki, Japan

ARTICLE INFO

Article history:
Received 12 August 2012
Returned to author for revisions
11 September 2012
Accepted 26 October 2012
Available online 19 November 2012

Keywords:
Canine distemper virus
Nectin4
Receptor
Morbillivirus

ABSTRACT

Recent outbreaks in monkeys have proven that canine distemper virus (CDV) causes diseases in a wide range of mammals. CDV uses SLAM and nectin4 as receptors to replicate in susceptible animals. Here, we show that human nectin4, but not human SLAM, is fully functional as a CDV receptor. The CDV Ac96I strain hardly replicated in nectin4-expressing human epithelial NCI-H358 cells, but readily adapted to grow in them. Unsurprisingly, no amino acid change in the H protein was required for the adaptation. The original Ac96I strain possessed a truncated C protein, and a subpopulation possessing the intact C protein was selected after growth in NCI-H358 cells. Other CDV strains possessing the intact C protein showed significantly higher growth abilities in NCI-H358 cells than the Ac96I strain with the truncated C protein. These findings suggest that the C protein is functional in human epithelial cells and critical for CDV replication in them.

Introduction

Distemper is an acute systemic infectious disease that mainly affects dogs and other canidae, and is caused by canine distemper virus (CDV) (Sawatsky et al., 2011). The disease is characterized by fever, coughing, vomiting, diarrhea, and neurological manifestations. CDV belongs to the genus *Morbillivirus* in the family *Paramyxoviridae*. Measles virus (MV), rinderpest virus, phocine distemper virus, Peste-des-petits-ruminants virus, and cetacean morbillivirus also belong to the genus, and cause severe acute systemic infections in humans, cows, seals, goats, and dolphins, respectively (Wang et al., 2012). The host range of these viruses is generally restricted to specific animal species. Recently, however, animals of many species, *Ailuridae* (Kotani et al., 1989), *Mustelidae* (Perpinan et al., 2008), *Viverridae* (Hirama et al., 2004; Hur et al., 1999), *Procyonidae* (Roscoe, 1993), *Phocidae* (Osterhaus et al., 1988), and *Felidae* (Appel et al., 1994; Roelke-Parker et al., 1996), have been naturally infected with CDV. Importantly, in the last several years, CDV has caused lethal outbreaks in nonhuman primates (Qiu et al., 2011; Sun et al., 2010).

Viruses in the genus *Morbillivirus* are enveloped viruses that possess a nonsegmented negative-stranded RNA genome encoding six genes, N, P/V/C, M, F, H, and L (Wang et al., 2012). The genome is encapsidated by the nucleocapsid (N) protein, forming a helical ribonucleocapsid that is associated with a viral RNA-dependent RNA polymerase composed of the phospho- (P) and large (L) proteins. In addition to the P protein, the P gene encodes two nonstructural proteins, V and C, by a process of RNA editing and an alternative translation initiation in a different reading frame, respectively (Wang et al., 2012). The V and C proteins are non-essential products, but play important roles in counteracting the host innate immune responses (Nakatsu et al., 2008; Rothlisberger et al., 2010; von Messling et al., 2006). On the envelope, there are two types of spike proteins, the hemagglutinin (H) and fusion (F) proteins. The H protein is responsible for receptor binding, while the F protein mediates membrane fusion between the viral envelope and the host cell plasma membrane. Both CDV and MV have been shown to use signaling lymphocyte activation molecule (SLAM) and nectin4 as receptors (Muhlebach et al., 2011; Noyce et al., 2011; Pratakpiriya et al., 2012; Seki et al., 2003; Tatsuo et al., 2000). SLAM is expressed on a subset of immune cells, while nectin4 is expressed at adherens junctions in the epithelial tissues of various organs (Takeda et al., 2011). Some neural cells in the central nervous system of dogs also

* Corresponding author. Fax: +81 42 562 8941.
E-mail address: otsuki@nih.go.jp (N. Otsuki).

0042-6822/$ - see front matter © 2012 Elsevier Inc. All rights reserved.
http://dx.doi.org/10.1016/j.virol.2012.10.033